*Department of Physics, Kyoto University*
*Yukawa Institute for Theoretical Physics*

KUNS 1405
YITP/96-31
September 7, 2018



# Scalar gravitational wave from Oppenheimer-Snyder collapse in scalar-tensor theories of gravity

Tomohiro Harada[1] *
Takeshi Chiba[2] †
Ken-ichi Nakao[1] ‡
Takashi Nakamura[2] §
[1] *Department of Physics, Kyoto University, Kyoto 606-01, Japan*
[2] *Yukawa Institute for Theoretical Physics, Kyoto University, Kyoto 606-01, Japan*

Unlike general relativity, scalar-tensor theories of gravity predict scalar gravitational waves even from a spherically symmetric gravitational collapse. We solve numerically the generation and propagation of the scalar gravitational wave from a spherically symmetric and homogeneous dust collapse under the approximation that we can neglect the back reaction of the scalar wave on the spacetime, and examine how the amplitude, characteristic frequency and waveform of the observed scalar gravitational wave depend on the initial radius and mass of the dust and parameters contained in the theory. In the Brans-Dicke theory, through the observation of the scalar gravitational wave, it is possible to determine the initial radius and mass and a parameter contained in the theory. In the scalar-tensor theories, it would be possible to determine the first derivative of the coupling function contained in the theory because the waveform of the scalar gravitational wave greatly depends on it.

PACS number(s): 04.30.-w, 04.50.+h, 04.80.Cc

## I. INTRODUCTION

Until now general relativity has passed all the test experiments in the solar system and pulsar-timing tests with high accuracy. However, general relativity is not the only gravitational theory that passes such tests. There are alternative theories of gravity that pass the present weak-field gravitational tests. In strong-field regime, these theories may deviate very widely from general relativity. Therefore experiments in strong-field regimes are necessary in order to determine the correct theory of gravity.

In the 1960's scalar-tensor theories of gravity were actively studied as alternative theories of gravity. Recently they have been revived. The reasons are that these theories may play an important role in the hyper-extended inflation model [1], that these theories arise naturally as the low-energy limit of string theory [2,3] or other unified theories, and that laser interferometric gravitational wave observatories (LIGO [4]) project will be in practical use next decade [5] and other projects (VIRGO [6], GEO [7] and TAMA [8]) of gravitational wave observations are being carried forward so that high-accuracy tests of the scalar-tensor theories may be expected [9,10].

In the scalar-tensor theories of gravity we consider scalar fields as well as a metric tensor as fields that are related to gravity. The scalar-tensor theories must agree with general relativity within an accuracy of at least $\sim 0.1\%$ in the weak-field region from the results of solar-system experiments and pulsar tests [11]. But a class of scalar-tensor

* e-mail: harada@tap.scphys.kyoto-u.ac.jp
† e-mail: chiba@yukawa.kyoto-u.ac.jp
‡ e-mail: nakao@tap.scphys.kyoto-u.ac.jp
§ e-mail: takashi@yukawa.kyoto-u.ac.jp

theories that satisfies the above constraints may predict order-of-magnitude deviations from general relativity in the regime of strong gravitational field [12]. One example of such phenomena in the strong-field regime may be the gravitational collapse of a star. The Brans-Dicke theory [13] is the well-known example of scalar-tensor theories. Collapse in the Brans-Dicke theory has been researched in comparison with that in general relativity. Matsuda and Nariai [14] studied a spherically symmetric collapse of ideal gas by numerical calculations of relativistic hydrodynamics in the Brans-Dicke theory. Shibata, Nakao and Nakamura [10] solved numerically a spherically symmetric collapse of inhomogeneous dust and examined the character of the gravitational collapse and the wave form of the radiated scalar gravitational wave. They found that the final state of the collapse is the Schwarzschild black hole, which is consistent with the theorem of Hawking [15] that a stationary black hole in the Brans-Dicke theory is identical with that of general relativity. Scheel, Shapiro and Teukolsky [16] found similar results to Shibata, Nakao and Nakamura [10].

Since in general relativity no gravitational wave is radiated from a spherically symmetric collapse, we cannot obtain any information of collapse from observations of gravitational waves if realistic gravitational collapses to black hole are almost spherically symmetric. However in scalar-tensor theories scalar gravitational waves are radiated even from spherically symmetric collapse and these scalar gravitational waves can be detected by laser interferometric gravitational wave detectors [10]. It is expected that these scalar gravitational waves reflect directly not only the stellar initial radius, mass and density but also the theory of gravity.

In this paper we take a spherically symmetric, homogeneous dust collapse as a model of the collapse of the stellar core and examine the scalar gravitational wave radiation and its wave form. As a first step to understand the nature of the scalar gravitational waves in general, we neglect the back reaction of the scalar field on the space-time in this paper. The method for numerical calculations is similar to that of Cunningham, Price and Moncrief [17]. We use null coordinates in order to see the propagation of the scalar gravitational wave.

This paper is organized as follows. In Sec.II we review scalar-tensor theories of gravity and scalar gravitational waves. In Sec.III we explicitly present our approximation and show the basic equations used in our numerical calculation . In Sec.IV we show numerical results and their implications. Sec.V will be devoted to discussions.

We use units of $c = 1$. The Greek indices $\mu, \nu, \cdots$ run over 0,1,2,3. A comma represents a partial derivative. We follow Misner, Thorne and Wheeler's [18] sign conventions of the metric tensor, Riemann tensor and Einstein tensor.

## II. SCALAR-TENSOR THEORY

### A. Field Equations

We consider a class of scalar-tensor theories of gravity in which gravitation is mediated by a mass-coupled, long-range scalar field in addition to space-time curvature. The action is given by [11]

$$I = \frac{1}{16\pi} \int \sqrt{-g} \left( \phi R - \frac{\omega(\phi)}{\phi} g^{\mu\nu} \phi_{,\mu} \phi_{,\nu} \right) d^4x + I_m[\Psi_m, g_{\mu\nu}], \tag{2.1}$$

where $g_{\mu\nu}$ is the metric tensor, $R$ is the scalar curvature, and $\phi$ is the scalar field that couples to gravity. $\phi$ approaches the cosmological value $\phi_0$ in the asymptotic region. $\omega(\phi)$ is a dimensionless arbitrary function of $\phi$. $\Psi_m$ represents matter fields, and $I_m$ is the action of them.

Varying the action by $g_{\mu\nu}$ and $\phi$ we have

$$\begin{aligned} R_{\mu\nu} - \frac{1}{2} g_{\mu\nu} R = {} & \frac{8\pi}{\phi} T_{\mu\nu} + \frac{\omega(\phi)}{\phi^2} \left( \phi_{,\mu} \phi_{,\nu} - \frac{1}{2} g_{\mu\nu} g^{\alpha\beta} \phi_{,\alpha} \phi_{,\beta} \right) \\ & + \frac{1}{\phi} (\nabla_\mu \nabla_\nu \phi - g_{\mu\nu} \Box \phi), \end{aligned} \tag{2.2}$$

$$\Box \phi = \frac{1}{3 + 2\omega(\phi)} \left( 8\pi T - \frac{d\omega}{d\phi} g^{\alpha\beta} \phi_{,\alpha} \phi_{,\beta} \right), \tag{2.3}$$

where $\nabla_\nu$ and $\Box$ are a covariant derivative and the d'Alembertian of $g_{\mu\nu}$ respectively. The equations of motion for matter fields are given by

$$\nabla_\nu T^{\mu\nu} = 0, \tag{2.4}$$

where the energy-momentum tensor $T^{\mu\nu}$ is defined by

$$T^{\mu\nu} \equiv \frac{2}{\sqrt{-g}} \frac{\delta I_m[\Psi_m, g_{\mu\nu}]}{\delta g_{\mu\nu}}. \tag{2.5}$$

The weak equivalence principle is valid in this theory: A test particle which has negligible self-gravitational energy moves on a geodesic in this frame, which is often called the Brans-Dicke frame or the Jordan-Fierz frame. However, a self-gravitating body moves on a different trajectory because of the coupling of the scalar field to the body's self-gravity and therefore the gravitational weak equivalence principle is not valid (Nordtvedt effect) [11,19].

In the asymptotic region, the gravitational "constant" $G_0$, which is measured in time dilation experiment or by observation of the Keplerian motion of a test particle, is given by [20]

$$G_0 = \phi_0^{-1} \frac{4 + 2\omega(\phi_0)}{3 + 2\omega(\phi_0)}. \tag{2.6}$$

Taking the units of $G_0 = 1$, we have

$$\phi_0 = \frac{4 + 2\omega(\phi_0)}{3 + 2\omega(\phi_0)}. \tag{2.7}$$

If $\omega(\phi)$ is a constant, the theory reduces to the Brans-Dicke theory. In the limit of $\omega \to \infty$, the theory approaches general relativity, although it does not mean that every solution of the theory approaches some solution of general relativity in this limit [16,21].

We can take another representation of the theory by the conformal transformation from the "physical" Brans-Dicke frame to the "unphysical" frame in which the Einstein-Hilbert action is separated from the scalar field action [22]. This new frame is often called the "Einstein" frame. In this frame, the action is [23]

$$I = \frac{1}{16\pi G_*} \int \sqrt{-g_*}(R_* - 2g_*^{\mu\nu}\varphi_{,\mu}\varphi_{,\nu})d^4x + I_m[\Psi_m, A^2(\varphi)g_{*\mu\nu}], \tag{2.8}$$

where $G_*$ is the "bare" gravitational constant and $\varphi$ is the scalar field. The metric tensor $g_{*\mu\nu}$ in the Einstein frame is related to the metric tensor $g_{\mu\nu}$ in the Brans-Dicke frame by the conformal transformation as

$$g_{\mu\nu} = A^2(\varphi)g_{*\mu\nu}. \tag{2.9}$$

$R_*$ is the scalar curvature of $g_{*\mu\nu}$. $\varphi$ and $A(\varphi)$ are determined by

$$G_* A^2(\varphi) = \frac{1}{\phi}, \tag{2.10}$$

$$\alpha^2(\varphi) = \frac{1}{3 + 2\omega(\phi)}, \tag{2.11}$$

where $\alpha(\varphi)$ is defined by

$$\alpha(\varphi) \equiv \frac{d \ln A(\varphi)}{d\varphi}. \tag{2.12}$$

The field equations are given by

$$G_{*\mu\nu} = R_{*\mu\nu} - \frac{1}{2}R_* g_{*\mu\nu} = 8\pi G_* T_{*\mu\nu} + 2\left(\varphi_{,\mu}\varphi_{,\nu} - \frac{1}{2}g_{*\mu\nu}g_*^{\alpha\beta}\varphi_{,\alpha}\varphi_{,\beta}\right), \tag{2.13}$$

$$\Box_*\varphi = -4\pi G_*\alpha(\varphi)T_*, \tag{2.14}$$

with the equations of motion given by

$$\nabla_{*\nu}T_{*\mu}^{\nu} = \alpha(\varphi)T_*\nabla_{*\mu}\varphi, \tag{2.15}$$

where $\nabla_{*\nu}$ , $\Box_*$ and $R_{*\mu\nu}$ are a covariant derivative , the d'Alembertian and the Ricci tensor of $g_{*\mu\nu}$, respectively. $T_*^{\mu\nu}$ is defined by

$$T^{*\mu\nu} \equiv \frac{2}{\sqrt{-g_*}} \frac{\delta I_m[\Psi_m, A^2(\varphi)g_{*\mu\nu}]}{\delta g_{*\mu\nu}}, \tag{2.16}$$

and is related to the energy-momentum tensor $T_{\mu\nu}$ in the physical Brans-Dicke frame by

$$T_{*\mu\nu} = A^2(\varphi) T_{\mu\nu}. \tag{2.17}$$

$\varphi$ approaches the cosmological value $\varphi_0$ in the asymptotic region. Hereafter we take the units $G_* = 1$ .

Generally, $\alpha(\varphi)$ is an arbitrary function that characterizes the theory. If $\alpha(\varphi)$ is constant, the theory reduces to the Brans-Dicke theory. In the limit $\alpha \to 0$ , the theory approaches general relativity. We denote

$$\alpha_0 \equiv \alpha(\varphi_0), \tag{2.18}$$

$$\beta_0 \equiv \left. \frac{d\alpha(\varphi)}{d\varphi} \right|_{\varphi=\varphi_0}. \tag{2.19}$$

In the post-Newtonian approximation, the PPN parameters $\gamma_{Edd}$ and $\beta_{Edd}$ are expressed as [23]

$$1 - \gamma_{Edd} = \frac{2\alpha_0^2}{1+\alpha_0^2}, \tag{2.20}$$

$$\beta_{Edd} - 1 = \frac{\beta_0 \alpha_0^2}{2(1+\alpha_0^2)^2}. \tag{2.21}$$

Results of solar-system test experiments (the time-delay and deflection of light) and pulsar-timing tests constrain $|1-\gamma_{Edd}|$ as [11,24]

$$|1 - \gamma_{Edd}| < 2 \times 10^{-3}. \tag{2.22}$$

This inequality is rewritten in terms of $\omega$ and $\alpha_0$ as

$$\omega > 500, \quad \alpha_0^2 < 10^{-3}. \tag{2.23}$$

The deviation of $\beta_{Edd}$ from unity implies the breakdown of the gravitational weak equivalence principle. Bounds on this effect from the results of the lunar-laser-ranging experiment constrain $\beta_{Edd} - 1|$ as [25]

$$|\beta_{Edd} - 1| \lesssim 7 \times 10^{-4}. \tag{2.24}$$

This constraint on $\beta_{Edd}$ comes only through the combination of $\alpha_0$ and $\beta_0$ in Eq.(2.21). Therefore the smaller the $\alpha_0$ is, the looser it constrains $\beta_0$. Very recently, Damour and Esposito-Farèse [26] found that binary-pulsar experiments constrain $\beta_0$ to

$$\beta_0 > -5, \tag{2.25}$$

independently of the value of $\alpha_0$ for a particular choice of the functional form $\alpha(\varphi)$.

### B. Scalar Gravitational Wave

We show that a scalar mode as well as tensor modes propagates as gravitational waves. We consider linear perturbations from the Minkowskian metric $\eta_{\mu\nu}$ and constant scalar field $\phi_0$.

$$g_{\mu\nu} = \eta_{\mu\nu} + h_{\mu\nu}, \tag{2.26}$$

$$\phi = \phi_0 + \delta\phi. \tag{2.27}$$

Hereafter in this section we raise and drop tensor indices by the flat metric $\eta^{\mu\nu}$ and $\eta_{\mu\nu}$. The field equations (2.2) and (2.3) in the linear perturbation are given by [13]

$$\begin{aligned} &\frac{1}{2}(h_\mu{}^\alpha{}_{,\nu\alpha} + h_\nu{}^\alpha{}_{,\mu\alpha} - h_{\mu\nu}{}^{,\alpha}{}_\alpha - h_{,\mu\nu}) - \frac{1}{2}\eta_{\mu\nu}(h_{\alpha\beta}{}^{,\alpha\beta} - h_{,\alpha}{}^{\alpha}) \\ &\quad = \frac{8\pi}{\phi_0} T_{\mu\nu} + \frac{1}{\phi_0}(\delta\phi_{,\mu\nu} - \eta_{\mu\nu}\Box\delta\phi), \end{aligned} \tag{2.28}$$

$$\Box\delta\phi = \frac{8\pi}{3+2\omega_0} T, \tag{2.29}$$

where $\omega_0 \equiv \omega(\phi_0)$ and $h \equiv h_\alpha{}^\alpha$.

We introduce

$$\theta_{\mu\nu} \equiv h_{\mu\nu} + \frac{\delta\phi}{\phi_0}\eta_{\mu\nu}. \tag{2.30}$$

Then Eqs.(2.28) and (2.29) become

$$\theta_{\mu\alpha,\nu}{}^{\alpha} + \theta_{\nu\alpha,\mu}{}^{\alpha} - \theta_{\mu\nu}{}^{,\alpha}{}_{\alpha} - \theta_{,\mu\nu} - \eta_{\mu\nu}(\theta_{\alpha\beta}{}^{,\alpha\beta} - \theta_{,\beta}{}^{\beta}) = \frac{16\pi}{\phi_0}T_{\mu\nu}, \tag{2.31}$$

$$\Box\delta\phi = \frac{8\pi}{3+2\omega_0}T, \tag{2.32}$$

where $\theta \equiv \theta_{\alpha}{}^{\alpha}$. We define $\bar{\theta}_{\mu\nu}$ and $\bar{h}_{\mu\nu}$ by

$$\bar{\theta}_{\mu\nu} \equiv \theta_{\mu\nu} - \frac{1}{2}\eta_{\mu\nu}\theta, \tag{2.33}$$

and

$$\bar{h}_{\mu\nu} \equiv h_{\mu\nu} - \frac{1}{2}\eta_{\mu\nu}h. \tag{2.34}$$

We use the gauge condition defined by

$$\bar{h}^{\mu\alpha}{}_{,\alpha} = \frac{\delta\phi^{,\mu}}{\phi_0}. \tag{2.35}$$

Then the field equations are separated as

$$\Box\bar{\theta}_{\mu\nu} = -\frac{16\pi}{\phi_0}T_{\mu\nu}, \tag{2.36}$$

$$\Box\delta\phi = \frac{8\pi}{3+2\omega_0}T. \tag{2.37}$$

In the absence of matter these equations are wave equations. We can use the remaining degrees of gauge freedom to make $\bar{\theta}_{\mu\nu}$ transverse-traceless. Then the metric perturbations are separated out into the plus mode, cross mode and scalar mode. The form of the metric perturbation of the plane wave is expressed by

$$h_{\mu\nu} = \begin{pmatrix} 0 & 0 & 0 & 0 \\ 0 & h_+ & h_\times & 0 \\ 0 & h_\times & -h_+ & 0 \\ 0 & 0 & 0 & 0 \end{pmatrix} - \frac{\delta\phi}{\phi_0}\begin{pmatrix} -1 & 0 & 0 & 0 \\ 0 & 1 & 0 & 0 \\ 0 & 0 & 1 & 0 \\ 0 & 0 & 0 & 1 \end{pmatrix}, \tag{2.38}$$

where $h_+$ , $h_\times$ represent the plus and cross mode, respectively. We can detect the scalar mode by a laser interferometric gravitational wave detector as shown by Shibata, Nakao and Nakamura [10]. If four detectors are available, we can distinguish the plus, cross and the scalar modes and determine the direction of the source in principle [10].

From Eqs.(2.10)-(2.12), we can relate the scalar field perturbation $\delta\phi = \phi - \phi_0$ in the Brans-Dicke frame to the scalar field perturbation $\delta\varphi = \varphi - \varphi_0$ in the Einstein frame in the linear approximation as

$$\delta\phi = -2\alpha_0(1+\alpha_0^2)\delta\varphi. \tag{2.39}$$

## III. BASIC EQUATIONS

### A. $\alpha_0$ Expansion

Hereafter we adopt the Einstein frame. We use the Taylor expansion of $\alpha(\varphi)$ that characterizes the coupling of the scalar field and matter as

$$\alpha(\varphi) = \alpha_0 + \beta(\varphi - \varphi_0) + \beta^{(2)}(\varphi - \varphi_0)^2 + \cdots, \tag{3.1}$$

where $\alpha_0$ represents a deviation of the theory from general relativity. We assume that $|\alpha_0| \ll 1$. Although it may exclude interesting non-perturbative effects, such as a *spontaneous scalarization* [12,26], we expand the metric tensor, scalar field and energy-momentum tensor of matters in terms of $\alpha_0$,

$$T_{*\alpha\beta} = T^{(E)}_{\alpha\beta} + \alpha_0 t^{(1)}_{\alpha\beta} + \alpha_0^2 t^{(2)}_{\alpha\beta} + O(\alpha_0^3), \tag{3.2}$$

$$g_{*\alpha\beta} = g^{(E)}_{\alpha\beta} + \alpha_0 h^{(1)}_{\alpha\beta} + \alpha_0^2 h^{(2)}_{\alpha\beta} + O(\alpha_0^3), \tag{3.3}$$

$$\varphi = \varphi_0 + \alpha_0 \varphi^{(1)} + \alpha_0^2 \varphi^{(2)} + O(\alpha_0^3). \tag{3.4}$$

From the lowest order of $\alpha_0$ in Eq.(2.13), we obtain

$$G^{(E)}_{\alpha\beta} = 8\pi T^{(E)}_{\alpha\beta}. \tag{3.5}$$

This means that $g^{(E)}_{\alpha\beta}$ and $T^{(E)}_{\alpha\beta}$ are solutions in general relativity. From the next order of $\alpha_0$, we obtain

$$G^{(1)}_{\alpha\beta} = 8\pi t^{(1)}_{\alpha\beta}. \tag{3.6}$$

This is also the same as the Einstein equations, so that the metric of the scalar-tensor theory deviates from the general relativity by $O(\alpha_0^2)$. Therefore we can determine the scalar field up to $O(\alpha_0)$ by solving the wave equation of the scalar field as

$$\Box^{(E)}\varphi = -4\pi\alpha(\varphi) T^{(E)}. \tag{3.7}$$

Back reaction of the scalar field on the space-time can be estimated from $O(\alpha_0^2)$ of Eq.(2.13) as

$$G^{(2)}_{\alpha\beta} = 8\pi t^{(2)}_{\alpha\beta} + 2\left(\varphi^{(1)}_{,\alpha}\varphi^{(1)}_{,\beta} - \frac{1}{2} g^{(E)}_{\alpha\beta} g^{(E)\mu\nu} \varphi^{(1)}_{,\mu}\varphi^{(1)}_{,\nu}\right). \tag{3.8}$$

This means that the back reaction can be neglected if relations

$$\varphi^{(1)} \sim O(1), \tag{3.9}$$

and

$$\alpha_0^2 |T^{(2)}_{\varphi\alpha\beta}| \ll |T^{(E)}_{\alpha\beta}|, \tag{3.10}$$

are satisfied. Here we have defined the energy-momentum tensor $T^{(2)}_{\varphi\alpha\beta}$ of the scalar field as

$$T^{(2)}_{\varphi\alpha\beta} \equiv \frac{1}{4\pi}\left(\varphi^{(1)}_{,\alpha}\varphi^{(1)}_{,\beta} - \frac{1}{2} g^{(E)}_{\alpha\beta} g^{(E)\mu\nu} \varphi^{(1)}_{,\mu}\varphi^{(1)}_{,\nu}\right). \tag{3.11}$$

### B. Oppenheimer-Snyder Collapse

We use the Oppenheimer-Snyder model [27] as the background space-time and matter in which the scalar field evolves. The Oppenheimer-Snyder solution describes a gravitational collapse of a homogeneous spherical dust ball.

In the interior of the dust one can write the line element in the closed Friedmann form

$$ds^2 = -d\tau^2 + a(\tau)^2 (d\chi^2 + \sin^2\chi d\Omega^2) \tag{3.12}$$

$$= a(\eta)^2 (-d\eta^2 + d\chi^2 + \sin^2\chi d\Omega^2), \tag{3.13}$$

$$d\Omega^2 = d\theta^2 + \sin^2\theta d\phi^2, \tag{3.14}$$

where

$$a(\eta) = \frac{1}{2} a_0 (1 + \cos\eta), \tag{3.15}$$

$$\tau(\eta) = \frac{1}{2} a_0 (\eta + \sin\eta). \tag{3.16}$$

The density of the dust is given by

$$\rho(\eta) = \frac{3a_0}{8\pi}a^{-3} = \frac{3}{8\pi {a_0}^2}\left\{\frac{1}{2}(1+\cos\eta)\right\}^{-3}. \tag{3.17}$$

The ranges of $\eta$ and $\chi$ are

$$0 \le \eta < \pi, \tag{3.18}$$

and

$$0 \le \chi \le \chi_0 < \frac{\pi}{2}. \tag{3.19}$$

Let $r_s(t)$ be the circumferential radius of the stellar surface. Then in the exterior of the dust ($r > r_s(t)$), the space-time is expressed by the Schwarzschild metric as

$$ds^2 = -\left(1-\frac{2M}{r}\right)dt^2 + \left(1-\frac{2M}{r}\right)^{-1}dr^2 + r^2 d\Omega^2. \tag{3.20}$$

The matching conditions of the interior and exterior solutions are that the proper circumference radius of stellar surface should agree and that the stellar surface should move on a geodesic. These matching conditions are expressed as

$$r_s = a(\eta)\sin\chi_0, \tag{3.21}$$

$$M = \frac{1}{2}a_0\sin^3\chi_0, \tag{3.22}$$

$$\begin{aligned} t = {} & 2M\ln\left|\frac{\left(\frac{r_{s0}}{2M}-1\right)^{\frac{1}{2}}+\tan\frac{\eta}{2}}{\left(\frac{r_{s0}}{2M}-1\right)^{\frac{1}{2}}-\tan\frac{\eta}{2}}\right| \\ & +2M\left(\frac{r_{s0}}{2M}-1\right)^{\frac{1}{2}}\left[\eta+\left(\frac{r_{s0}}{4M}\right)(\eta+\sin\eta)\right], \end{aligned} \tag{3.23}$$

where $r_{s0} \equiv r_s(t=0)$.

### C. Wave Equation

We rewrite Eq.(3.7) under the background of the Oppenheimer-Snyder collapse. We use the metric in the form (3.14) and (3.20). The wave equation in the interior ( $0 \le \chi \le \chi_0$) is given by

$$\frac{1}{a^2}\left\{-\frac{1}{a^2}\frac{\partial}{\partial\eta}\left(a^2\frac{\partial\delta\varphi}{\partial\eta}\right)+\frac{1}{\sin^2\chi}\frac{\partial}{\partial\chi}\left(\sin^2\chi\frac{\partial\delta\varphi}{\partial\chi}\right)\right\} = 4\pi\alpha(\varphi)\rho, \tag{3.24}$$

while in the exterior ($r > r_s(t)$) it is given by

$$-\left(1-\frac{2M}{r}\right)^{-1}\frac{\partial^2\delta\varphi}{\partial t^2}+\frac{1}{r^2}\frac{\partial}{\partial r}\left\{r^2\left(1-\frac{2M}{r}\right)\frac{\partial\delta\varphi}{\partial r}\right\} = 0. \tag{3.25}$$

Here in place of $\delta\varphi$ we define $\zeta$ by

$$\zeta \equiv \begin{cases} a\sin\chi\delta\varphi & \text{(interior)} \\ r\delta\varphi & \text{(exterior).} \end{cases} \tag{3.26}$$

Substituting Eq.(3.26) into Eqs.(3.24) and (3.25) , we have

$$-\frac{\partial^2\zeta}{\partial\eta^2}+\frac{\partial^2\zeta}{\partial\chi^2} = -\left(1+\frac{a''}{a}\right)\zeta + 4\pi\alpha(\varphi)\rho a^3\sin\chi \quad \text{(interior)}, \tag{3.27}$$

$$-\frac{\partial^2\zeta}{\partial t^2}+\frac{\partial^2\zeta}{\partial r_*^2} = \frac{2M}{r^3}\left(1-\frac{2M}{r}\right)\zeta \quad \text{(exterior)}, \tag{3.28}$$

where $r_*$ is the tortoise coordinate defined by

$$r_* = r + 2M \ln\left(\frac{r}{2M} - 1\right), \tag{3.29}$$

and the prime stands for differentiation with respect to $\eta$. Using the null coordinates, we can rewrite Eqs.(3.27) and (3.28) as

$$\frac{\partial^2 \zeta}{\partial u \partial v} = \frac{1}{4}\left(1 + \frac{a''}{a}\right)\zeta - \frac{3}{8}\alpha(\varphi) a_0 \sin\chi \quad \text{(interior)}, \tag{3.30}$$

$$\frac{\partial^2 \zeta}{\partial \tilde{u} \partial \tilde{v}} = -\frac{M}{2r^3}\left(1 - \frac{2M}{r}\right)\zeta \quad \text{(exterior)}, \tag{3.31}$$

where the null coordinates are defined by

$$u = \eta - \chi, \tag{3.32}$$

$$v = \eta + \chi, \tag{3.33}$$

in the interior and

$$\tilde{u} = t - r_*, \tag{3.34}$$

$$\tilde{v} = t + r_*, \tag{3.35}$$

in the exterior, and we have used Eqs.(3.15) and (3.17) to rewrite $a''$ and $\rho$.

The boundary condition at the center of the dust is that the derivative of the scalar field in the radial direction should be zero, *i.e.*,

$$\frac{\partial \delta\varphi}{\partial \chi} = 0 \quad \text{at} \quad \chi = 0. \tag{3.36}$$

The junction condition on the stellar surface is that $\varphi$ and its derivative in the direction normal to the boundary surface should be continuous, *i.e.*,

$$\delta\varphi|_{in} = \delta\varphi|_{ex}, \tag{3.37}$$

$$n^\mu \delta\varphi_{,\mu}|_{in} = n^\mu \delta\varphi_{,\mu}|_{ex}, \tag{3.38}$$

at $\chi = \chi_0$ (interior) and $r = r_s(t)$ (exterior), where $n^\mu$ is the normal vector to the boundary surface of the dust.

For simplicity we take the initial condition that $\varphi = \varphi_0$ and the time derivative of $\varphi$ vanishes on the initial hypersurface $\eta = 0$ and $t = 0$. Namely in the interior of the dust we set

$$\delta\varphi = 0, \tag{3.39}$$

$$\frac{\partial \delta\varphi}{\partial \eta} = 0, \tag{3.40}$$

at $\eta = 0$ , and in the exterior of the dust

$$\delta\varphi = 0, \tag{3.41}$$

$$\frac{\partial \delta\varphi}{\partial t} = 0, \tag{3.42}$$

on the first ray $\tilde{u} = \tilde{u}_0 \equiv -r_{*s}(t=0)$, because $\varphi = \varphi_0$ is the static solution in the exterior region that satisfies the boundary condition in the asymptotic region. We can regard this as the initial condition of the situation that for $t < 0$ a highly relativistic star is in equilibrium between the pressure and the gravity, and at $t = 0$ the pressure is switched off and the homogeneous dust begins to collapse, because, for highly relativistic matter, the trace of the energy-momentum tensor satisfies

$$T = -\rho + 3P = 0. \tag{3.43}$$

## IV. NUMERICAL RESULTS

We divide the Oppenheimer-Snyder space-time to three regions (A), (B) and (C) as shown in Fig.1 according to Cunningham, Price and Moncrief [17]. We use null coordinates in the numerical calculation in order to observe propagation of the scalar field to the asymptotic region. The details of our numerical calculation will be described in Appendix A. As for the coupling function, for simplicity, we assume that

$$\alpha(\varphi) = \alpha_0 + \beta(\varphi - \varphi_0). \tag{4.1}$$

### A. Brans-Dicke Theory

#### *1. Wave Form in the Wave Zone*

We shall see the behavior of the scalar field in the Brans-Dicke theory (*i.e.*, $\beta = 0$) to obtain an overall picture of the time evolution of the scalar field. Fig.2 shows the wave form of the scalar gravitational wave by an observer at $r = 100M$ in the Brans-Dicke theory from the collapse of the dust whose initial radius $r_{s0}$ is $10M$. The ordinate is $\zeta = r\delta\varphi$. The solution is proportional to the parameter $\alpha_0$ and hereafter we shall normalize $\zeta$ by $\alpha_0 = -0.0316$ corresponding to $\omega = 500$. The first ray reaches the present observer at $t \sim 95M$ and then the scalar field increases from the initial value $\varphi_0$ to the peak. The amplitude at the peak is estimated as [10]

$$\delta\varphi \sim \frac{\alpha_0 M}{r}. \tag{4.2}$$

After the peak, the value of the scalar field $\varphi$ decreases below the initial constant asymptotic value $\varphi_0$ and increases monotonically toward $\varphi_0$. A frequency of this last bounce below $\varphi_0$ nearly equals that of the spherically symmetric, fundamental quasi-normal mode [28]. This result is in a good agreement with Shibata, Nakao and Nakamura's result of full numerical simulations [10]. This also shows that the back reaction of the scalar field on the space-time can be neglected when $\omega + 3/2 \gtrsim 5$, *i.e.*, $|\alpha_0| \lesssim 0.316$.

#### *2. Time Evolution of the Scalar Field*

Next we shall see the numerical solution $\zeta$ in the interior of the dust (the region (A)). The result is shown in Figs.3(a-c). Fig.3(a) shows the scalar field in the interior of the dust (the region (A)) in Fig.1. The initial dust radius $r_{s0}$ is 10M. The case of the initial radius $r_{s0} = 10M$ is very instructive and therefore we shall first consider this case. The abscissas are the null coordinates $u = \eta - \chi$ and $v = \eta + \chi$. Fig.3(b) shows the time evolution of the scalar field seen by comoving observers. The abscissa is the conformal time $\eta$ and the numbers attached to the curves are the values of the fixed radial coordinates $\chi$ of the comoving observers. Fig.3(c) shows the time evolution of the scalar field configuration on the spacelike hypersurface of the conformal time $\eta = const.$. The abscissa is the radial coordinate $\chi$ and the numbers attached to the curves are the value of $\eta$.

As already mentioned, at $\eta = 0$ the scalar field is $\varphi_0$, i.e., $\zeta = 0$ everywhere. Then $\varphi$ increases homogeneously in the central region ($u \sim v$) because the source of the scalar field is the *homogeneous* dust ball and the information of the surface of the dust ball has not yet arrived at the central region in the early stage. The information from the surface of the dust ball propagates inward at the speed of light and reaches the center at the time $\eta = \chi_0$. After the reflection at the center, the configuration of the scalar field in the interior of the dust settles to a *quasi-static solution* ($\partial\zeta/\partial\eta \sim 0$) along the outgoing null ray $u \sim \chi_0$ and after that the scalar field evolves in a quasi-static manner. Finally the scalar field falls inside the event horizon, keeping its value finite.

In Sec.IV A 3, we will see that the quasi-static configuration is realized only when the initial radius of the dust ball is large enough. This fact suggests that the quasi-static evolution appears in the case $\chi_0 \ll 1$, which means that the gravity is weak in the initial configuration. In order to confirm this expectation, we shall assume that $\chi_0 \ll 1$ and that the interior solution $\zeta = \zeta_{in}$ can be expanded with respect to $\chi_0$. Then we can obtain a consistent quasi-static solution up to $O(\chi_0^3)$, which is given by

$$\zeta_{in} = \frac{1}{4}\alpha_0 a_0 \chi(\chi^2 - 3\chi_0^2), \tag{4.3}$$

$$\zeta_{ex} = -\frac{1}{2}\alpha_0 a_0 \chi_0^3 \sim -\alpha_0 M. \tag{4.4}$$

The derivation of this solution will be described in Appendix C. We plot the interior solution (4.3) in Fig.3(c) with the label "QS". We see that the approximate solution agrees with the numerical solutions very well for the case of $\beta = 0$ even when the dust surface is rather close to the event horizon. When the surface of the dust ball is close to the event horizon, the amplitude of the scalar field in the interior region is

$$\delta\varphi \sim -\frac{\alpha_0 M}{r_s}, \tag{4.5}$$

and the ratio of the energy density of the scalar field to that of the dust remains $O(\alpha_0^2)$.

The numerical solution $\zeta = r\delta\varphi$ in the exterior of the dust is shown in Figs.4 (the region (B)) and 5 (the region (C)). The set of null coordinates $u$ , $v$ of Fig.4 is a continuous extension of the interior characteristic coordinates obtained by relabeling the rays $\tilde{u} = const.$ and $\tilde{v} = const.$. The details of this coordinate extension will be described in Appendix B. In the region (B) the scalar field increases and settles to the quasi-static configuration on the null ray $u \sim \chi_0$. In the region (C) the outgoing radiation of the scalar field can be seen. If we retrieve $G$ and $c$, the units of time and length become

$$\frac{GM}{c^3} = 4.93 \times 10^{-6} \frac{M}{M_\odot} \quad \text{sec}, \tag{4.6}$$

$$\frac{GM}{c^2} = 1.48 \frac{M}{M_\odot} \quad \text{km}, \tag{4.7}$$

respectively.

As seen in Figs.4 and 5, first the scalar field increases from the initial value $\varphi_0$ due to the presence of the dust. When the event horizon is formed, the field inside cannot affect the field outside. At that moment no wave propagates outwardly from the region (B) to the region (C). In the wave zone the scalar field approaches the asymptotic value $\varphi_0$ after the wave has passed the observer at $r = const.$. This is consistent with the Hawking's theorem which states that the black hole has no scalar charge [15]. In Fig.5 a steep cliff can be seen on the boundary $\tilde{v} = \tilde{v_0}$ between the regions (B) and (C) but this is only due to the coordinate singularity of the Schwarzschild coordinates and does not mean any singular behavior of the scalar field.

### *3. Dependence on the Initial Radius of the Dust*

In Fig.6, wave forms of the scalar gravitational waves from the collapse of the dust whose initial radii $r_{s0}$ are $3M$, $4M$, $6M$, $8M$, $10M$ and $20M$ in the Brans-Dicke theory are plotted. As we can see in Fig.6, peaks are nearly symmetric for $r_{s0} \lesssim 4M$ but not for $r_{s0} \gtrsim 4M$. Fig.7 shows the relation between the peak amplitude of the wave form and the initial dust radius. As seen from Fig.7 , the amplitudes at the peaks are nearly $|\alpha_0|M/r$ for $r_{s0} \gtrsim 4M$ but smaller than $|\alpha_0|M/r$ for $r_{s0} \lesssim 4M$. These can be explained as follows. The information on the stellar surface reaches the center of the dust first at $\eta = \chi_0$. On the other hand the information at the center at $\eta \geq \pi - 3\chi_0$ cannot travel to the exterior because it is inside the event horizon. Therefore for the dust of $\chi_0 \gtrsim \pi/4$, *i.e.*, $r_{s0} \lesssim 4M$, the scalar field cannot reach the quasi-static evolution until the event horizon is formed. So a mild downhill after the peak, which is an evidence of the quasi-static evolution in the interior of the dust , cannot be seen for $r_{s0} \lesssim 4M$. On the other hand, for $r_{s0} \gtrsim 4M$, a mild down hill after the peak implies the quasi-static evolution in the interior of the dust.

For $r_{s0} \gtrsim 4M$, since the initial ingoing null ray from the stellar surface bounces back to the surface $\eta \sim 2\chi_0$, the time $\Delta t_{peak}$ that it takes for the scalar field to reach the peak from its rise is estimated as

$$\begin{aligned}\Delta t_{peak} &\sim t(\eta = 2\chi_0) \\ &= 2M \ln \left| \frac{\cot\chi_0 + \tan\chi_0}{\cot\chi_0 - \tan\chi_0} \right| \\ &+ 2M \cot\chi_0 \left[ 2\chi_0 + \frac{1}{2\sin^2\chi_0}(2\chi_0 + \sin 2\chi_0) \right].\end{aligned} \tag{4.8}$$

This shows an agreement with the numerical results in Fig.6 within an accuracy of $\sim$ 10 %. For example, using Eq.(4.8), we can estimate $\Delta t_{peak}$ to be $\sim 40M$ for $r_{s0} = 20M$.

Fig.8 shows the relation between an initial dust radius $r_{s0}$ and a characteristic frequency $f_c$ which is defined as the frequency at which the energy spectrum of the wave form takes the maximal value. For $r_{s0} \gtrsim 8M$, the characteristic frequency $f_c$ is approximately in proportion to the inverse of the free-fall time of the initial dust, which is shown by Shibata, Nakao and Nakamura [10] as

$$f_c \propto \frac{1}{t_{ff}} \sim \sqrt{\rho_0}. \tag{4.9}$$

For $r_{s0} \lesssim 8M$, though there is no such simple relation because of the effect of the space-time curvature, $f_c$ would be determined by the initial radius and mass of the dust. The last bounce below the asymptotic value $\varphi_0$ reflects a quasi-normal oscillation. Fig.9 shows the relation between the initial dust radius and the time scale of the bounce, which is defined as the half value width of that bounce. As shown in Fig.9, the time scale of this bounce is almost independent from the initial dust radius and nearly equals to the period of the quasi-normal oscillation [28].

### B. Dependence of the results on the Parameter in the Theory

In Figs.10-12 the wave forms of the scalar gravitational waves seen by an observer at $r = 100M$ are shown, for various $\beta$, from the collapse of the dust whose initial radius is fixed to $10M$. In each figure, the scalar field approaches the asymptotic value after the peak, the quasi-normal mode of the scalar wave having passed the point of the observer, which is consistent with the black hole no hair conjecture [29].

First we consider the case of positive $\beta$. The amplitude of the scalar gravitational wave decreases as $\beta$ increases. As seen from Figs.10 and 11 there appears another oscillation mode whose frequency is characteristic of the relevant gravitational theory and the dust density. The larger $\beta$ is, the shorter is the period of this oscillation mode and the more the scalar field oscillates before it approaches the asymptotic value. This can be also seen from Fig.13, which shows the time of the first minimum from the reach of the first ray. This oscillation mode reflects an oscillation mode in the interior of the dust seen in Fig.14, which shows the time evolution of the scalar field observed by comoving observers in the region(A) for $\beta = 50$ . The ratio of the energy density of the scalar field to that of the dust remains within $\sim O(\alpha_0^2)$. So, if $|\alpha_0| \ll 1$, the back reaction of the scalar field on the space-time is negligible.

Second we consider the case of negative $\beta$. The amplitude of the scalar wave increases as $|\beta|$ increases, as seen in Fig.12. This reflects an exponential growth of the scalar field in the interior of the dust seen in Fig.15, which shows the time evolution of the scalar field observed by comoving observers in the region(A) for $\beta = -5$ . The ratio of the energy of the scalar field to that of the dust is $\sim 10 \times O(\alpha_0^2)$ for $\beta = -1$, $\sim 100 \times O(\alpha_0^2)$ for $\beta = -5$ and $\sim 10^4 \times O(\alpha_0^2)$ for $\beta = -10$. Therefore, if we consider a finite value of $\alpha_0$, there is a critical value of $\beta$ for which the back reaction of the scalar field cannot be neglected.

As we have seen in Sec.II A, in fact, the solar-system test experiments for the post-Newtonian order deviation from general relativity do not constrain directly the value of $\beta$ because $\beta$ is constrained only through the combination with $\alpha_0$ in Eq.(2.21) (however, see [26]). So the wave form for $\beta$, the value of which is allowed by the solar-system experiments, may be quite different from that in the Brans-Dicke theory.

## V. DISCUSSIONS AND SUMMARY

In the Brans-Dicke theory the peak amplitude of the scalar gravitational wave is given by

$$\delta\phi \sim \alpha_0 \delta\varphi \sim 10^{-23} \left(\frac{500}{\omega}\right) \left(\frac{M}{M_\odot}\right) \left(\frac{10\text{Mpc}}{r}\right), \tag{5.1}$$

and the characteristic frequency is given by

$$f_c \sim 3 \times 10^3 \left(\frac{M}{M_\odot}\right) \left(\frac{r_{s0}}{15\text{km}}\right)^{-\frac{3}{2}} \text{Hz} \tag{5.2}$$

if $r_{s0} \gtrsim 4M$. For this frequency the sensitivity of the first LIGO would be $h \sim 10^{-21}$ and that of the advanced LIGO would be $h \sim 10^{-22}$. If $\omega \sim 500$, the advanced LIGO may detect the scalar gravitational wave from collapse of a nearly spherical mass $\sim 1M_\odot$ and initial radius $\sim 15$km at the distance $\sim 1$Mpc from us. If the delayed collapse [30,31] after a supernova would happen in our Galaxy, we can test the Brans-Dicke theory by the advanced LIGO up to $\omega \lesssim 10^5$. Even for a neutron star formation, scalar gravitational wave may be emitted because the progenitor would lose a considerable part of its scalar mass in the process. The amplitude of the wave would tell us the information of its self-gravitational energy. If a wave form of the scalar gravitational wave from gravitational collapse is obtained observationally, we can determine its amplitude, characteristic frequency and quasi-normal mode frequency. We can then determine the source mass because the frequency of the quasi-normal mode is in proportion to the inverse of the mass. If we know, in addition, the distance to the source by another method, we can determine the Brans-Dicke parameter $\omega$. Moreover, we can determine the initial dust radius from its characteristic frequency. In the case of delayed collapse after the supernova, the core radius would correspond to it. The information of the initial radius would constrain the possible high-density equation of state.

Next we consider the parameter dependence of the wave form in the scalar-tensor theory. The wave form greatly depends on $\beta$. If the space-time is flat and the density is homogeneous, a homogeneous solution which describes harmonic oscillations at the period $\sqrt{\pi/(\beta\rho)}$ for $\beta > 0$ and an exponential increase at the $e$-fold time $1/(2\sqrt{\pi|\beta|\rho})$ for $\beta < 0$ appears. Such a mode would appear in the wave form of the scalar gravitational wave. For $\beta > 0$ the back reaction of the scalar field on the space-time is negligible, and so we can safely expand the theory around general relativity. Therefore we can determine the wave form of the scalar gravitational wave within our approximation. For $\beta < 0$ the back reaction is not negligible and the full calculation that deals with the dynamics of the metric, matter and scalar field is needed in order to predict the correct wave form [32]. We also see in Eq.(3.7) that the scalar field gets an effective mass $m^2 = -4\pi\beta T$. For $\beta > 0$, the scalar field can be regarded as being effectively massive since $T = -\rho + 3P < 0$ , and for $\beta < 0$, the scalar field gets effectively a *tachyonic* mass.

Finally we make a crude estimate of the condition in which the scalar mode of gravitational waves radiated from its collapse dominates over the tensor mode. We consider collapse of an oblate spheroid of mass $M$. Then the tensor mode of the wave at distance $r$ takes the form

$$h_T \simeq \frac{2}{r}\ddot{Q} \simeq \frac{2}{r}M(a^2 - c^2)^{\cdot\cdot}, \tag{5.3}$$

where $a$ and $c$ are the semi -major axis and semi-minor axis respectively. While the scalar mode is

$$h_S \simeq \frac{1}{\omega}\frac{M}{r}, \tag{5.4}$$

where $Q$ is the reduced quadrupole moment and the dot means a time derivative. If we replace the time derivative with the free-fall time $t_{ff}$, then the ratio of $h_T$ to $h_S$ is

$$h_T/h_S \sim \frac{2\omega}{M}\frac{M(a^2-c^2)}{t_{ff}^2} \sim 16\omega(a^2-c^2)\frac{M}{a^2 c} \sim 10^3\left(\frac{\omega}{500}\right)\left(\frac{10M}{a}\right)\frac{e^2}{\sqrt{1-e^2}}. \tag{5.5}$$

For example, for $\omega = 500$ and $a = 10M$ the scalar mode dominates over the tensor mode if the eccentricity $e \lesssim 0.03$. Thus the scalar mode would dominate in almost spherical collapse.

We have examined a scalar gravitational wave from a spherically symmetric and homogeneous dust collapse in the Brans-Dicke theory and scalar-tensor theories of gravity, where we have neglected the back reaction of the scalar field on the space-time.

(1) In the Brans-Dicke theory the back reaction of the scalar field on the space-time remains $\sim O(1/\omega)$. So if $\omega \gg 1$, it is negligible.

(2) In the Brans-Dicke theory the amplitude of the scalar gravitational wave is given by $\sim M/(\omega r)$ and the characteristic frequency is given by $\sim 3 \times 10^3 (M/M_\odot)^{-1}(r_{s0}/15\text{km})$Hz. The characteristic frequency of the scalar gravitational wave is in proportion to the inverse of the free-fall time of the initial dust sphere. The last bounce reflects the fundamental quasi-normal mode of the black hole. If $r_{s0} \gtrsim 4M$, the scalar field in the interior of the dust reaches a quasi-static configuration and thereafter evolves quasi-statically. Therefore the wave form after the peak goes down slowly. If $r_{s0} \lesssim 4M$, the scalar field in the interior of the dust does not reach the quasi-static configuration and so the wave form after the peak goes down more quickly. The peak amplitude of the scalar gravitational wave is smaller than $M/(\omega r)$ in this case.

(3) Both in the Brans-Dicke theory and in the scalar-tensor theory given by Eq.(4.1), the scalar field approaches its asymptotic value after the scalar wave radiation has passed the observer at $r = const.$. In our numerical calculation we did not find any singularity in the scalar field at the event horizon.

(4) In the Brans-Dicke theory we can determine a mass, initial radius of the dust and the Brans-Dicke parameter from the wave form of the scalar gravitational wave and the distance to its source.

(5) We calculated the scalar gravitational wave from the dust collapse in the scalar-tensor theory given by Eq.(4.1). The wave form greatly depends on the parameter $\beta$. If $\beta > 0$, the amplitude of the scalar gravitational wave is suppressed and a new oscillation mode whose time scale is $\sim 1/\sqrt{\beta\rho}$ appears. The back reaction of the scalar field on the space-time is within $\sim O(\alpha_0^2)$. If $\beta < 0$, the amplitude of the scalar gravitational wave is enhanced and its back reaction would not be negligible. Hence we have to solve the whole field equations fully numerically, which is the subject of our next paper [32].

## ACKNOWLEDGMENTS

We would like to thank T. Damour for suggesting to investigate this problem. We would like to thank M.Siino, M.Shibata, S.Hayward, Y.Fujii and H.Sato for useful discussions. T.H. and T.C. are also grateful to H.Sato for continuous encouragement. This work was in part supported by the Grant-in-Aid for Basic Research (No.08NP0801) and for Encouragement of Young Scientists (No.08740341) of Ministry of Education, Culture, Science and Sports.

## APPENDIX A: NUMERICAL CODE

The wave equations we have calculated take the following form.

$$\frac{\partial q}{\partial u} = A(u, v, \xi, p, q) \tag{A1}$$

$$\frac{\partial \xi}{\partial u} = p \tag{A2}$$

$$\frac{\partial p}{\partial v} = A(u, v, \xi, p, q) \tag{A3}$$

$$\frac{\partial \xi}{\partial v} = q \tag{A4}$$

Our numerical code is similar to that of Hamadé and Stewart [33], but we modified slightly their finite differential equations. We solve simultaneous partial differential equations given by

$$\frac{\partial y}{\partial u} = F(y, z) \tag{A5}$$

$$\frac{\partial z}{\partial v} = G(y, z). \tag{A6}$$

We determine $y_n$, $z_n$ at the point $\mathbf{n}(u, v)$ when $y_w$ and $z_w$ are given at the point $\mathbf{w}(u, v-h)$ and $y_e$, $z_e$ at the point $\mathbf{e}(u-h, v)$. At the first step we calculate

$$\hat{y_n} = y_e + hF(y_e, z_e) \tag{A7}$$

$$\hat{z_n} = z_w + \frac{1}{2}h(G(y_w, z_w) + G(\hat{y_n}, \hat{z_n})), \tag{A8}$$

and at the second step we calculate

$$y_n = \frac{1}{2}(\hat{y_n} + y_e + hF(\hat{y_n}, \hat{z_n})) \tag{A9}$$

$$z_n = \frac{1}{2}\left\{\hat{z_n} + z_w + \frac{1}{2}h(G(y_w, z_w) + G(\hat{y_n}, \hat{z_n}))\right\}. \tag{A10}$$

In general this is an implicit scheme, but since the right hand side of the wave equation we have calculated does not contain any first derivative of the field as seen Eqs.(3.30), (3.31), it becomes an explicit scheme. The error of the one set of these two steps is estimated as $O(h^3)$.

This code was checked through the following tests. We calculated a spherically symmetric, ingoing wave in flat space-time which bounces at the center, and compared it with an analytic solution. The error of this test is within $\sim 0.5\%$. We calculated scalar gravitational waves from the Oppenheimer-Snyder collapse in the Brans-Dicke theory and compared them to the results for $\omega = 500$ of the full simulation by Shibata, Nakao and Nakamura [10]. The two results are agreed within an accuracy of several percent. These tests made us sure that our numerical code works well. It took about two hours to compute one model by Panastation SS20.

## APPENDIX B: COORDINATE EXTENSION

It is convenient for our numerical calculation to divide the exterior region into the two regions (B) and (C) in Fig.1 by the inward light ray $\tilde{v} = \tilde{v}_0$ which reaches the stellar surface on the event horizon. We extend the interior comoving coordinates to the exterior region following Cunningham, Price and Moncrief [17]. We relabel light rays $\tilde{u} = const.$ and $\tilde{v} = const.$ by the interior coordinates $u$, $v$ at which these light rays reach the stellar surface. This coordinate transformation is expressed explicitly as

$$\tilde{u} = t_s(u+\chi_0) - r_{*s}(u+\chi_0), \tag{B1}$$

$$\tilde{v} = t_s(v-\chi_0) + r_{*s}(v-\chi_0), \tag{B2}$$

$$t_s(\eta) = 2M \ln \left| \frac{\cot\chi_0 + \tan\frac{\eta}{2}}{\cot\chi_0 - \tan\frac{\eta}{2}} \right| + 2M \cot\chi_0 \left[ \eta + \frac{1}{2\sin^2\chi_0}(\eta + \sin\eta) \right], \tag{B3}$$

$$r_{*s}(\eta) = a(\eta)\sin\chi_0 + 2M \ln \left| \frac{a(\eta)\sin\chi_0}{2M} - 1 \right|. \tag{B4}$$

This new coordinates are well-behaved everywhere in the space-time except for the central singularity of the space-time.

In these coordinates, the junction conditions on the surface become particularly simple because the vector normal to the surface is given

$$\mathbf{n} = \frac{1}{a}\left( \frac{\partial}{\partial v} - \frac{\partial}{\partial u} \right). \tag{B5}$$

## APPENDIX C: QUASI-STATIC SOLUTION

We assume that $\chi_0 \ll 1$ and that the interior solution $\zeta = \zeta_{in}$ can be expanded with respect to $\chi_0$ as

$$\zeta_{in} = \sum_{n=1}^{\infty} \zeta_{in}^{(n)}, \tag{C1}$$

where $\zeta_{in}^{(n)} = O(\chi_0^n)$. Since $\chi$ is small, the interior solution $\zeta_{in}$ will be well approximated by the truncated Taylor series of $\chi$ and therefore we should impose

$$\frac{\partial^m \zeta_{in}^{(n)}}{\partial \chi^m} = O(\chi_0^{n-m}). \tag{C2}$$

Under the assumption of the quasi-static evolution phase, $\partial\zeta_{in}/\partial\eta = \partial^2\zeta_{in}/\partial\eta^2 = 0$, the wave equation (3.27), in the case of $\beta = 0$, is written up to $O(\chi_0^5)$ as

$$\frac{\partial^2 \zeta_{in}^{(0)}}{\partial\chi^2} = 0, \tag{C3}$$

$$\frac{\partial^2 \zeta_{in}^{(1)}}{\partial\chi^2} = 0, \tag{C4}$$

$$\frac{\partial^2 \zeta_{in}^{(2)}}{\partial\chi^2} = -\frac{a_0}{2a}\zeta_{in}^{(0)}, \tag{C5}$$

$$\frac{\partial^2 \zeta_{in}^{(3)}}{\partial\chi^2} = -\frac{a_0}{2a}\zeta_{in}^{(1)} + \frac{3}{2}\alpha_0 a_0 \chi, \tag{C6}$$

$$\frac{\partial^2 \zeta_{in}^{(4)}}{\partial\chi^2} = -\frac{a_0}{2a}\zeta_{in}^{(2)}, \tag{C7}$$

$$\frac{\partial^2 \zeta_{in}^{(5)}}{\partial\chi^2} = -\frac{a_0}{2a}\zeta_{in}^{(3)} - \frac{1}{4}\alpha_0 a_0 \chi^3, \tag{C8}$$

where we have used Eqs.(3.15) and (3.17) to rewrite $a''$ and $\rho$.

On the other hand, we consider only the nontrivial, lowest-order solution for the exterior region. Since $2M/r_s = (a_0/a)\sin^2\chi_0 = O(\chi_0^2)$, as long as $a_0/a$ is not so large, the lowest order wave equation for the exterior solution $\zeta = \zeta_{ex}$ becomes

$$-\frac{\partial^2\zeta_{ex}}{\partial t^2} + \frac{\partial^2\zeta_{ex}}{\partial r^2} = 0. \tag{C9}$$

Under the assumption of quasi-static evolution, the matching condition between the interior and the exterior solutions at the dust surface $r = r_s$, that is, $\chi = \chi_0$ is given by

$$\zeta_{ex} = \zeta_{in}, \tag{C10}$$

$$\frac{\partial\zeta_{ex}}{\partial t} = \frac{1}{a}\sin\chi_0\sqrt{\frac{a_0}{a}-1}\frac{\partial\zeta_{in}}{\partial\chi} \sim \frac{1}{a}\sqrt{\frac{a_0}{a}-1}\frac{\partial\zeta_{in}}{\partial\chi}[\chi_0 + O(\chi_0^3)], \tag{C11}$$

$$\frac{\partial\zeta_{ex}}{\partial r} = \frac{1}{a}\left(1-\frac{a_0}{a}\sin^2\chi_0\right)^{-1}\cos\chi_0\frac{\partial\zeta_{in}}{\partial\chi} \sim \frac{1}{a}\frac{\partial\zeta_{in}}{\partial\chi}[1 + O(\chi_0^2)]. \tag{C12}$$

From the above equation, we find that

$$\frac{|\partial\zeta_{ex}/\partial t|}{|\partial\zeta_{ex}/\partial r|} = O(\chi_0) \qquad \text{at} \qquad r = r_s. \tag{C13}$$

This means that the exterior solution satisfies $\partial\zeta_{ex}/\partial t = 0$ in the lowest order of $\chi_0$ as long as $a_0/a \ll 1/\chi_0$ and therefore from Eq.(C9), we obtain

$$\zeta_{ex} = C_{ex} = const., \tag{C14}$$

where we have imposed the boundary condition $\zeta_{ex} \to const.$ for $r \to \infty$. From the above equation, the matching condition (C12) in the lowest order becomes

$$\frac{\partial\zeta_{in}}{\partial\chi} = 0 \qquad \text{at} \qquad \chi = \chi_0. \tag{C15}$$

Now we return to the interior solution. The solutions for $\zeta_{in}^{(n)}$ $(n = 0, 1)$ are given by

$$\zeta_{in}^{(0)} = C_{in}^{(0)} \qquad \text{and} \qquad \zeta_{in}^{(1)} = C_{in}^{(1)} + D_{in}^{(1)}\chi, \tag{C16}$$

where $C_{in}^{(n)}$ $(n = 0, 1)$ and $D_{in}^{(1)}$ are the integration constants and the order of those are, respectively, $C_{in}^{(0)}$, $D_{in}^{(1)} = O(1)$, $C_{in}^{(1)} = O(\chi_0)$. However from the regularity at the origin, $\chi = 0$, i.e., $\zeta_{in} \propto \chi$ for $\chi \to 0$, $C_{in}^{(0)}$ and $C_{in}^{(1)}$ vanish, while $D_{in}^{(1)}$ is determined by the matching condition (C15) and we find $D_{in}^{(1)}$ also vanishes. As a result, we get

$$\zeta_{in}^{(0)} = 0 = \zeta_{in}^{(1)}, \tag{C17}$$

Using the above results, we obtain the solutions of the equation for $\zeta_{in}^{(n)}$ $(n = 2, 3)$ as

$$\zeta_{in}^{(2)} = 0, \qquad \text{and} \qquad \zeta_{in}^{(3)} = \frac{1}{4}\alpha_0 a_0\chi^3 + D_{in}^{(3)}\chi, \tag{C18}$$

where we have used the regularity condition at the origin and $D_{in}^{(3)}$ is the integration constant which is determined by the matching condition (C15). Hence the non-trivial solution for the interior region appears at $O(\chi_0^3)$ and using this solution, $C_{ex}$ is determined from Eq.(C10). Then we obtain the solution given by Eqs.(4.3) and (4.4). This solution is clearly time independent and is consistent with the assumption of quasi-static evolution. From Eq.(C7), the first equation of Eq.(C18) and the regularity at the origin, we obtain $\zeta_{in}^{(4)} = 0$, while Eq.(C8) for $\zeta_{in}^{(5)}$ becomes

$$\frac{\partial^2\zeta_{in}^{(5)}}{\partial\chi^2} = -\frac{a_0^2}{8a}\alpha_0\chi(\chi^2 - 3\chi_0^2) - \frac{1}{4}\alpha_0 a_0\chi^3. \tag{C19}$$

The above equation shows that $\zeta_{in}^{(5)}$ depends on time $\eta$ through the first term in R.H.S. and hence the assumption of the quasi-static evolution is no longer consistent with the solution above $O(\chi_0^5)$. In the case of $\beta \neq 0$, the quasi-static solution (4.3), (4.4) is also valid up to $O(\chi_0^4)$. Here we should again note that our approximation based on the smallness of $\chi_0$ is valid only when $a_0/a$ is not so large, i.e., $a_0/a \ll 1/\chi_0$ and further $a_0/(2a) \ll 1/\chi_0^3$.

[1] P.J. Steinhardt and F.S. Accetta, Phys. Rev. Lett. **64**, 2740 (1990).
[2] C.G. Callan, D. Friedan, E.J. Martinec and M.J. Perry, Nucl. Phys. B **262**, 593 (1985).
[3] T. Damour and A.M. Polyakov, Nucl. Phys. B **423**, 532 (1994); Gen. Relativ. Gravit. **26**, 1171 (1994).
[4] A. Abramovici, *et al.,* Science **256**, 325 (1992).
[5] K.S. Thorne, in the *Proceedings of the International Conference on Particle Physics, Astrophysics and Cosmology* (Stanford Linear Accel. Centre, 1996), p.41.
[6] C. Bradaschia, *et al.,* Nucl. Instrum. and Methods A **289**, 518 (1990).
[7] J. Hough, in the *Proceedings of the Sixth Marcel Grossmann Meeting*, edited by H. Sato and T. Nakamura (World Scientific, Singapore, 1992), p.192.
[8] K. Kuroda, *et al.,* in the *Proceedings of International Conference on Gravitational Waves: Sources and Detectors*, Pisa, Italy, March 19-23, 1996 (in press).
[9] C.M. Will, Phys. Rev. D **50**, 6058 (1994).
[10] M. Shibata, K. Nakao and T. Nakamura, Phys. Rev. D **50**, 7304 (1994).
[11] C.M. Will, *Theory and Experiment in Gravitational Physics* (Rev. Ed., Cambridge University Press, Cambridge, 1993).
[12] T. Damour and G. Esposito-Farèse, Phys. Rev. Lett. **70**, 2220 (1993).
[13] C. Brans and R.H. Dicke, Phys. Rev. **124**, 925 (1961).
[14] T. Matsuda and H. Nariai, Prog. Theor. Phys. **49**, 1195 (1972).
[15] S.W. Hawking, Commun. Math. Phys. **25**, 167 (1971).
[16] M.A. Scheel, S.L. Shapiro and S.A. Teukolsky, Phys. Rev. D **51**, 4236 (1995).
[17] C.T. Cunningham, R.H. Price and V. Moncrief, Astrophys. J. **224**, 643 (1978).
[18] C.W. Misner, K.S. Thorne and J.A. Wheeler, *Gravitation* (W.H. Freeman and Company, New York, 1973).
[19] K. Nordtvedt, Phys. Rev. **169**, 1017 (1968).
[20] H.W. Zaglauer, Astrophys. J. **393**, 685 (1992).
[21] C. Romero and A. Barros, Phys. Lett. A **173**, 243 (1993).
[22] R.H. Dicke, Phys. Rev. **125**, 2163 (1962).
[23] T. Damour and K. Nordtvedt, Phys. Rev. D **48**, 3436 (1993).
[24] C.M. Will, **gr-qc/9602001**, Matters of Gravity (7), 8 (1996).
[25] J.O. Dickey, *et al.,* Science **265**, 482 (1994).
[26] T. Damour and G. Esposito-Farèse, Phys. Rev. D. **54**, 1474 (1996).
[27] J.R. Oppenheimer and H. Snyder, Phys. Rev. **56**, 455 (1939).
[28] N. Andersson, Proc. R. Soc. Lond. A **439**, 47 (1992).
[29] R. Ruffini and J.A. Wheeler, Phys. Today **24**, 30 (1971).
[30] G.E. Brown, S.W. Bruenn and J.C. Wheeler, Commun. Astrophys. **16**, 153 (1992).
[31] H.A. Bethe and G.E. Brown, Astrophys. J. **423**, 659 (1994); Astrophys. J. Lett. **445**, L129 (1995).
[32] T. Chiba, T. Harada, K. Nakao and T. Nakamura, in preparation.
[33] R.S. Hamadé and J.M. Stewart, Class. Quantum Grav. **13**, 497 (1996).

## FIGURE CAPTION

Fig.1. Regions of the Oppenheimer-Snyder space-time for constant $\theta$ and $\phi$, expressed in characteristic coordinates. In the "stationary region" the initial stationary field configuration remains a stationary solution.

Fig.2. The wave form of the scalar gravitational wave in the Brans-Dicke theory at $r = 100M$. The initial dust radius $r_{s0}$ is $10M$. The ordinate is $\zeta = r\delta\varphi$. The abscissa is the time $t$ from the beginning of the collapse at $t = 0$.

Fig.3. The scalar field in the interior of the dust (the region (A) of Fig.1) in the Brans-Dicke theory. The initial dust radius $r_{s0}$ is $10M$. (a) The ordinate is $\zeta = a \sin\chi\delta\varphi$. The abscissas are the null coordinates $u = \eta - \chi$ and $v = \eta + \chi$. (b) The time evolution of the scalar field seen by comoving observers. The numbers attached to the curves are the radial coordinates $\chi$ of the comoving observers. The ordinate is $\zeta = a \sin\chi$ and the abscissa is the conformal time $\eta$. (c) The scalar field configuration on the spacelike hypersurface of the conformal time $\eta = const.$. The abscissa is the radial coordinate $\chi$. The numbers attached to the curves are the value of $\eta$. The curve with the label "QS" shows the approximate quasi-static solution obtained in the text. See the text for further details.

Fig.4. The scalar field in the exterior of the dust (the region (B) of Fig.1) in the Brans-Dicke theory. The initial dust radius $r_{s0}$ is 10M. The ordinate is $\zeta = r\delta\varphi$. The abscissas are the null coordinates $u$ and $v$ extended from the interior region to the exterior.

Fig.5. The scalar field in the exterior of the dust (the region (C) of Fig.1) in the Brans-Dicke theory. The initial dust radius $r_{s0}$ is 10M. The ordinate is $\zeta = r\delta\varphi$. The abscissas are the null coordinates $\tilde{u} = t - r_*$ and $\tilde{v} = t + r_*$.

Fig.6. The wave forms of the scalar gravitational waves from the collapses of various initial radii in the Brans-Dicke theory. The ordinate and abscissa are the same as Fig.5. The numbers attached the curves represent the value of the initial radii respectively.

Fig.7. Relation between the peak amplitude and initial dust radius $r_{s0}$ in the Brans-Dicke theory.

Fig.8. Relation between the characteristic frequency $f_c$ and initial dust radius $r_{s0}$ in the Brans-Dicke theory.

Fig.9. Relation between the time scale of the last bounce and initial dust radius $r_{s0}$. The ordinate is the time scale of the last oscillation which is defined as the half-value width of that bounce.

Fig.10. The wave form of the scalar gravitational wave for various $\beta$ at $r = 100M$. The numbers attached to the curves represent the value of $\beta$ respectively.The initial dust radius $r_{s0}$ is fixed to $10M$.

Fig.11. Same as Fig.10, but for different $\beta$.

Fig.12. Same as Fig.10, but for different $\beta$.

Fig.13. The time of the first minimum of the wave form from the reach of the first ray as a function of $\beta > 0$.

Fig.14. The time evolution of the scalar field seen by comoving observers in the interior of the dust (the region (A) of Fig.1) for $\beta = 50$ . The ordinate and abscissa are same as Fig.3(b).

Fig.15. The time evolution of the scalar field seen by comving observers in the interior of the dust (the region (A) of Fig.1) for $\beta = -5$ . The ordinate and abscissa are same as Fig.3(b).

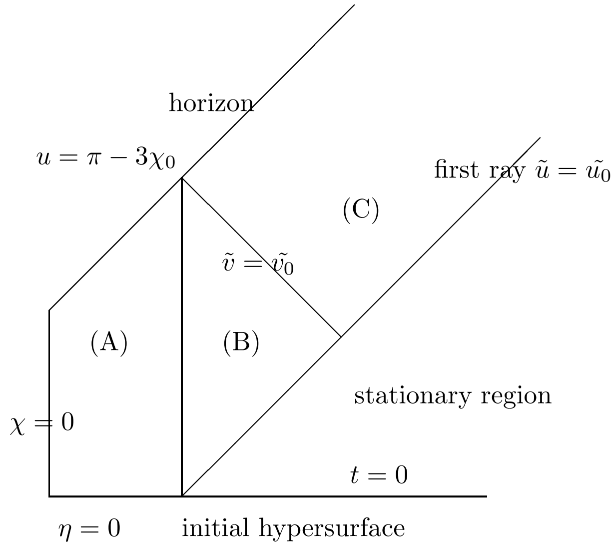
horizon
$u = \pi - 3\chi_0$
first ray $\tilde{u} = \tilde{u_0}$
(C)
$\tilde{v} = \tilde{v_0}$
(A)
(B)
stationary region
$\chi = 0$
$t = 0$
$\eta = 0$
initial hypersurface

Fig.1

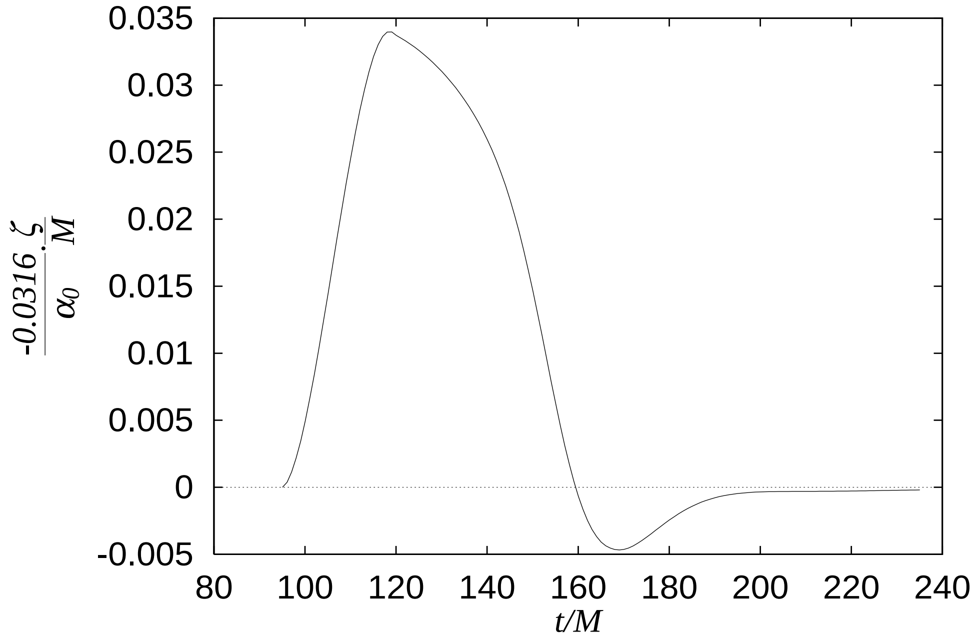
0.035
0.03
0.025
0.02
0.015
0.01
0.005
0
-0.005
80
100
120
140
160
180
200
220
240
$t/M$
$\frac{-0.0316}{\alpha_0} \cdot \frac{\zeta}{M}$

Fig.2

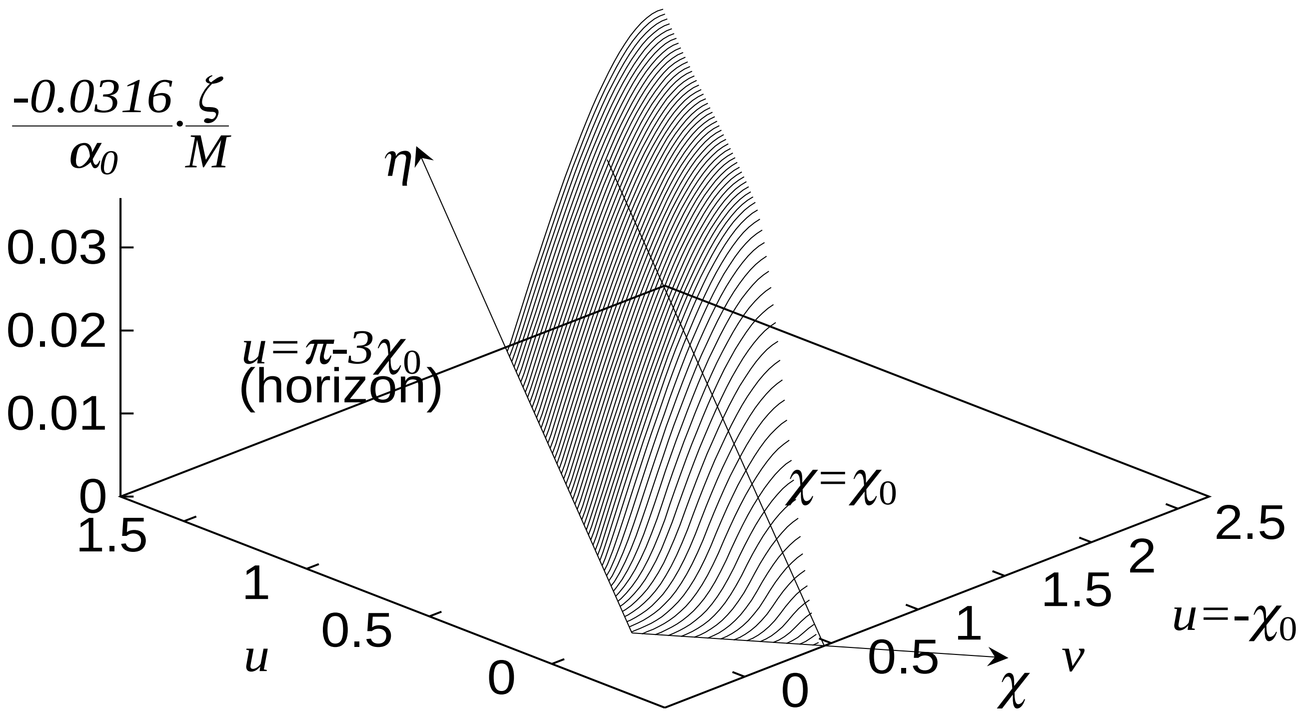
-0.0316/α0 · ζ/M
η
0.03
0.02
0.01
0
u=π-3χ0
(horizon)
χ=χ0
1.5
1
0.5
0
u
0
0.5
1
1.5
2
2.5
v
χ
u=-χ0

Fig.3(a)

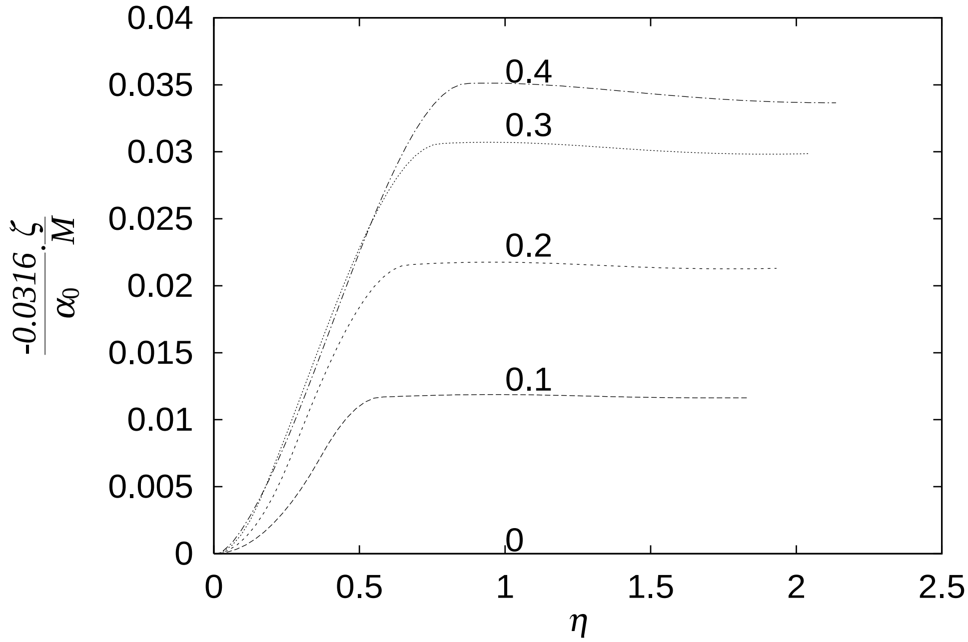


Fig.3(b)

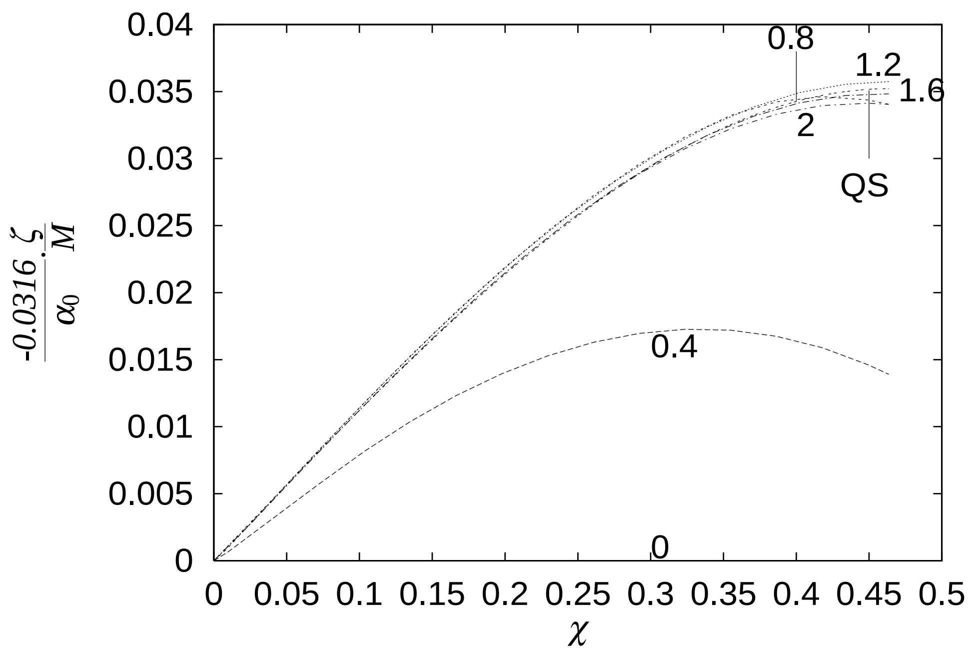


Fig.3(c)

Fig.4

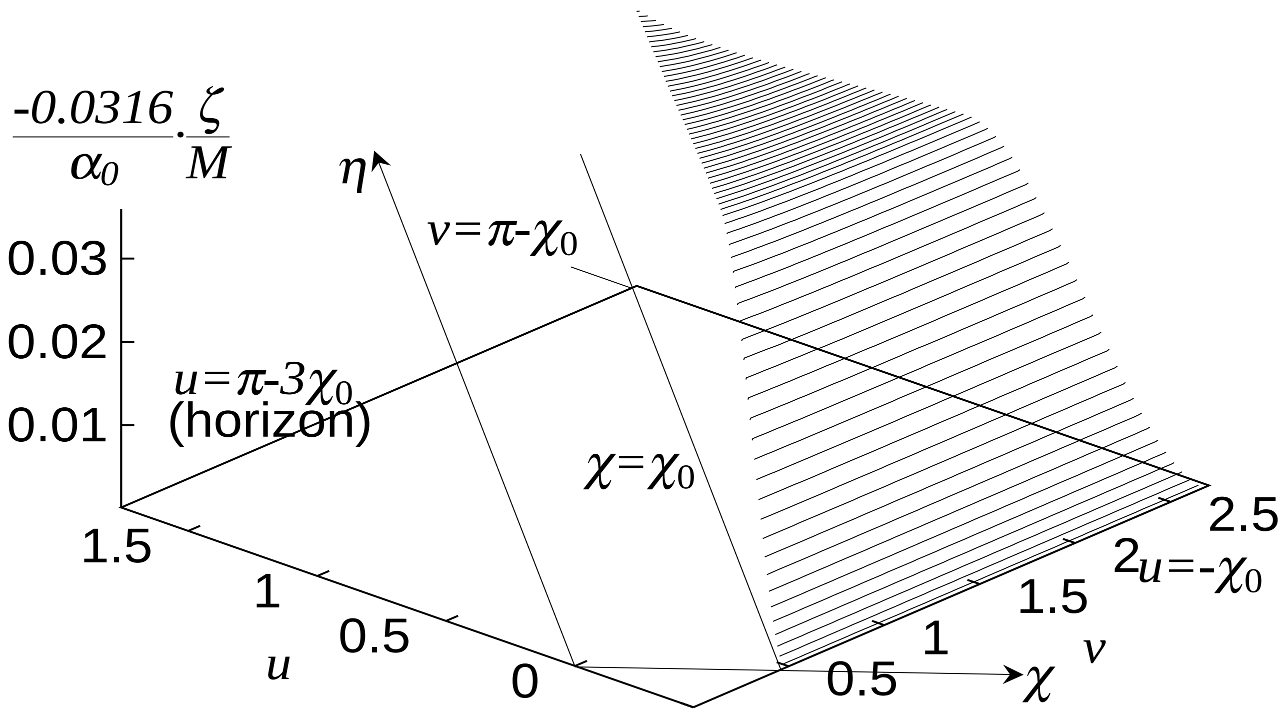
$\frac{-0.0316}{\alpha_0} \cdot \frac{\zeta}{M}$
0.03
0.02
0.01
$\eta$
$v=\pi-\chi_0$
$u=\pi-3\chi_0$
(horizon)
$\chi=\chi_0$
1.5
1
0.5
0
$u$
0.5
1
1.5
2
2.5
$u=-\chi_0$
$v$
$\chi$

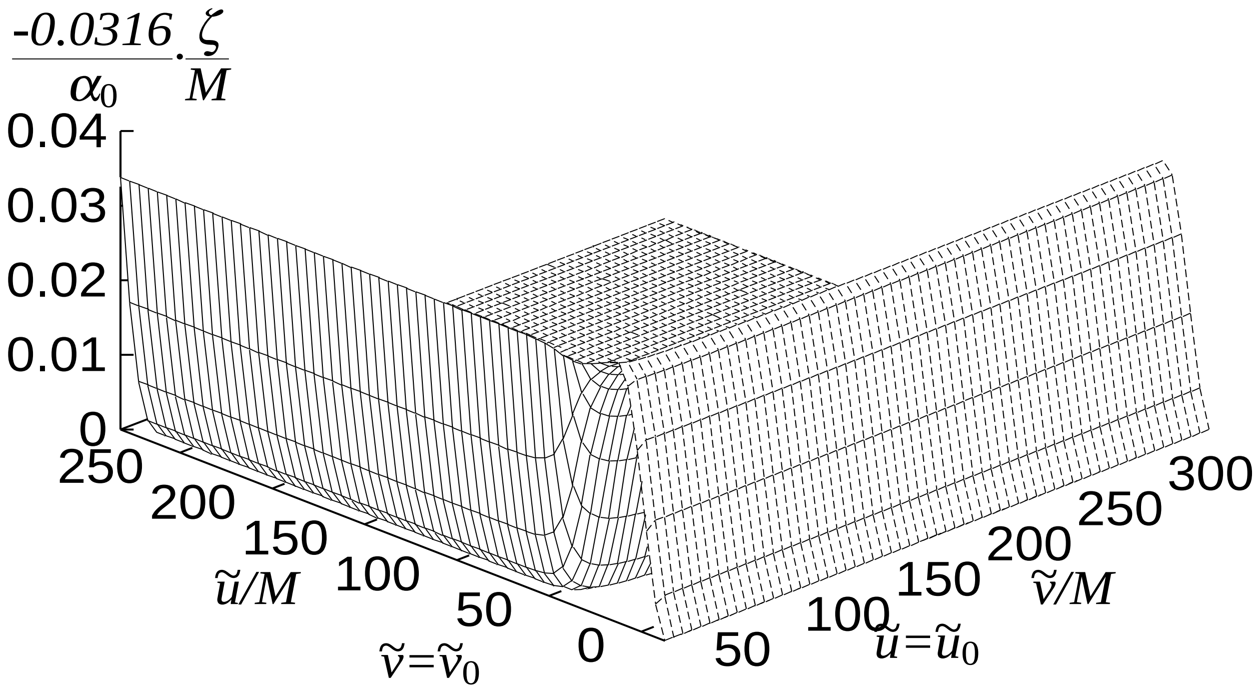

$\frac{-0.0316}{\alpha_0} \cdot \frac{\zeta}{M}$
0.04
0.03
0.02
0.01
0
250
200
150
100
50
0
$\tilde{u}/M$
$\tilde{v}=\tilde{v}_0$
50
100
150
200
250
300
$\tilde{v}/M$
$\tilde{u}=\tilde{u}_0$


Fig.5

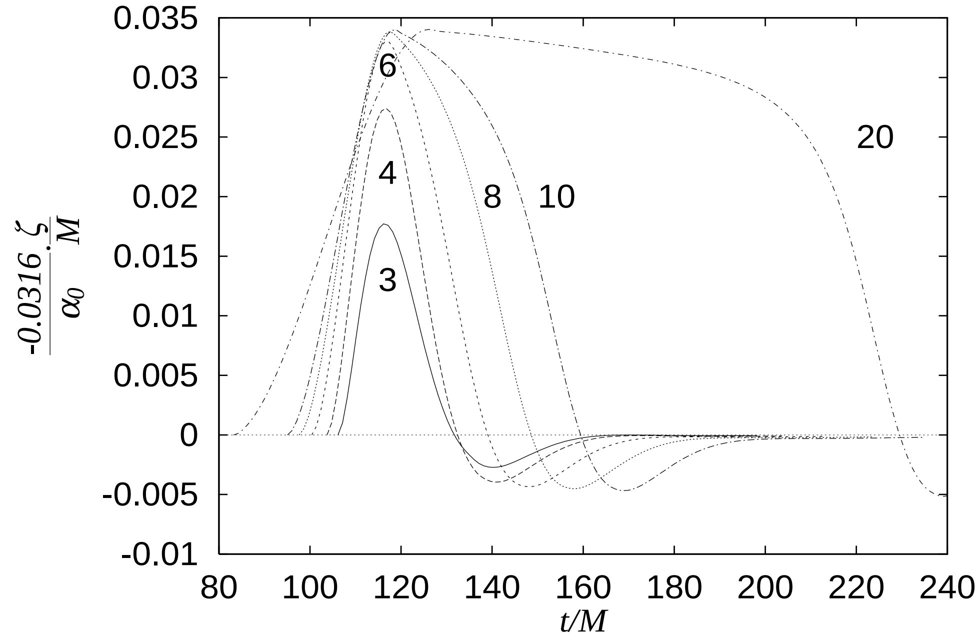

0.035
0.03
0.025
0.02
0.015
0.01
0.005
0
-0.005
-0.01
80
100
120
140
160
180
200
220
240
t/M
-0.0316 ζ / α0 · M
6
4
3
8
10
20


Fig.6

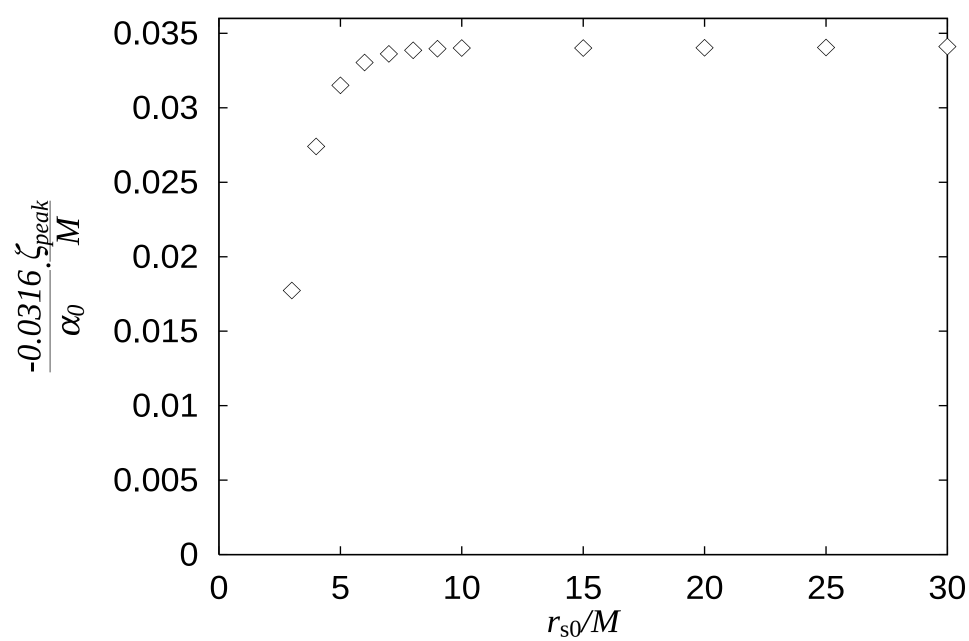

0.035
0.03
0.025
0.02
0.015
0.01
0.005
0
0
5
10
15
20
25
30
rs0/M
-0.0316 ζpeak / α0 · M


Fig.7

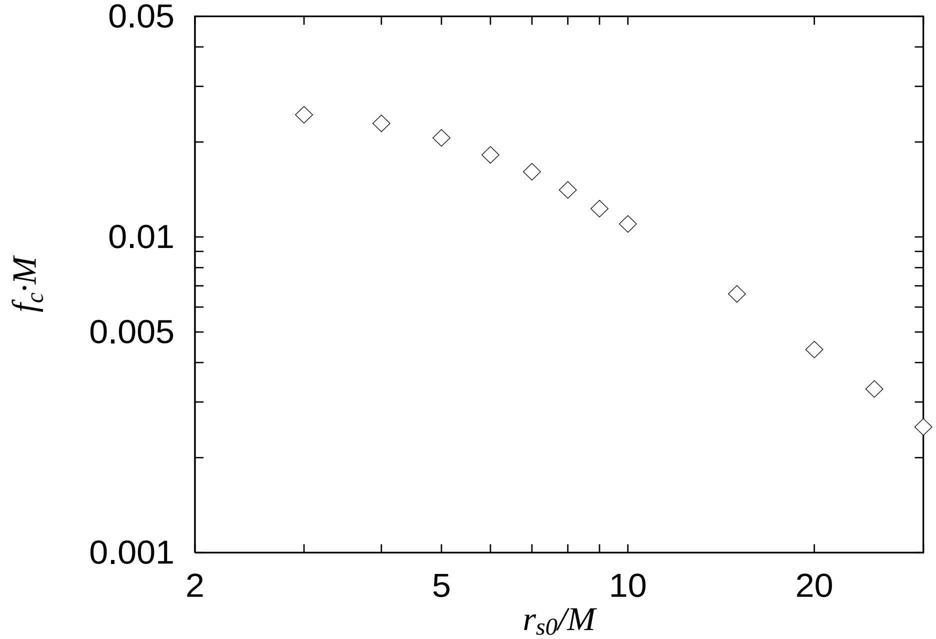
0.05
0.01
0.005
0.001
$f_c \cdot M$
2
5
10
20
$r_{s0}/M$

Fig.8

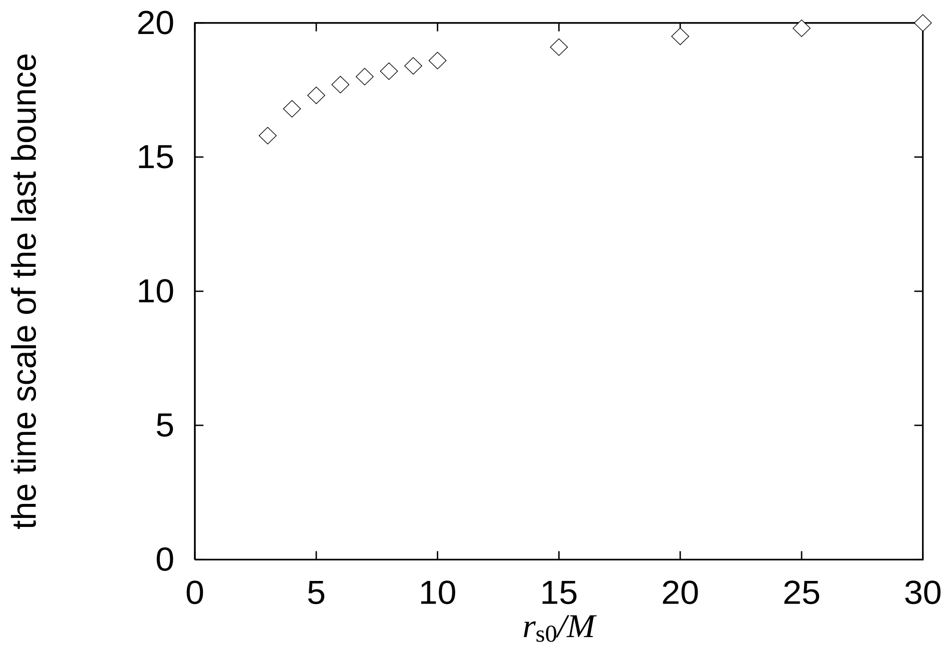
20
15
10
5
0
the time scale of the last bounce
0
5
10
15
20
25
30
$r_{s0}/M$

Fig.9

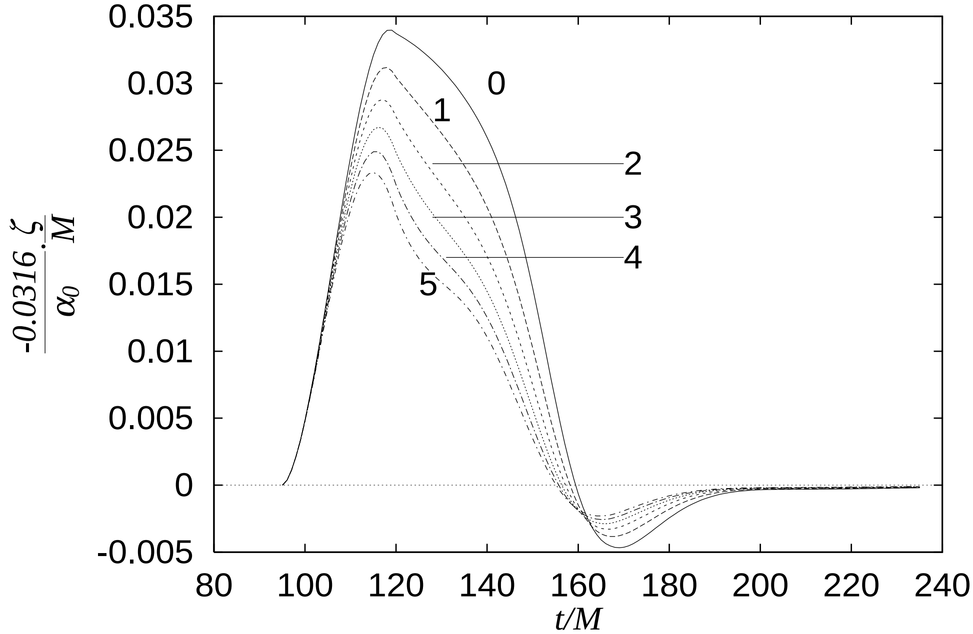
0.035
0.03
0.025
0.02
0.015
0.01
0.005
0
-0.005
80
100
120
140
160
180
200
220
240
t/M
0
1
2
3
4
5

Fig.10

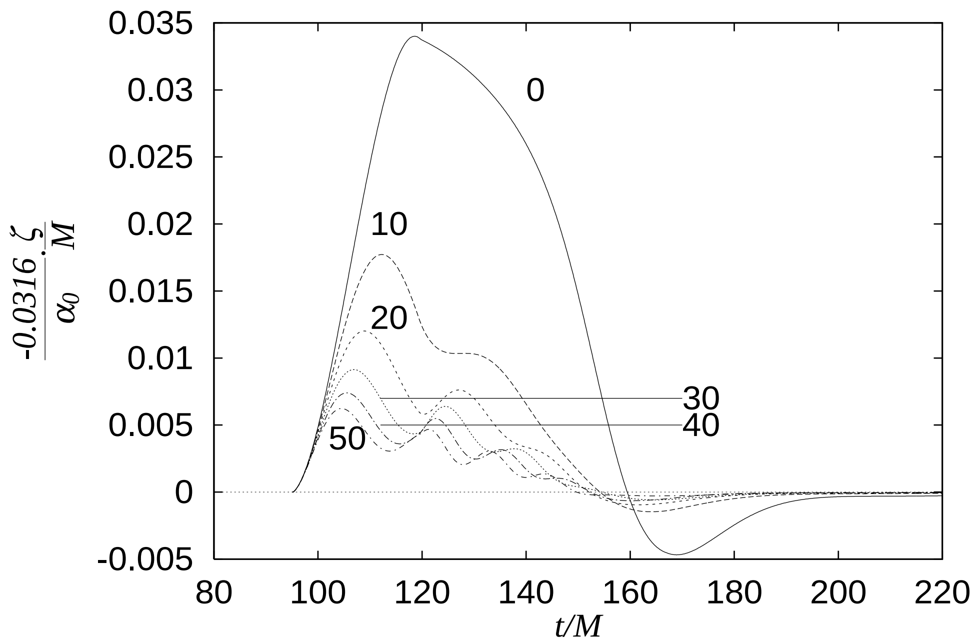
0.035
0.03
0.025
0.02
0.015
0.01
0.005
0
-0.005
80
100
120
140
160
180
200
220
t/M
0
10
20
30
40
50

Fig.11

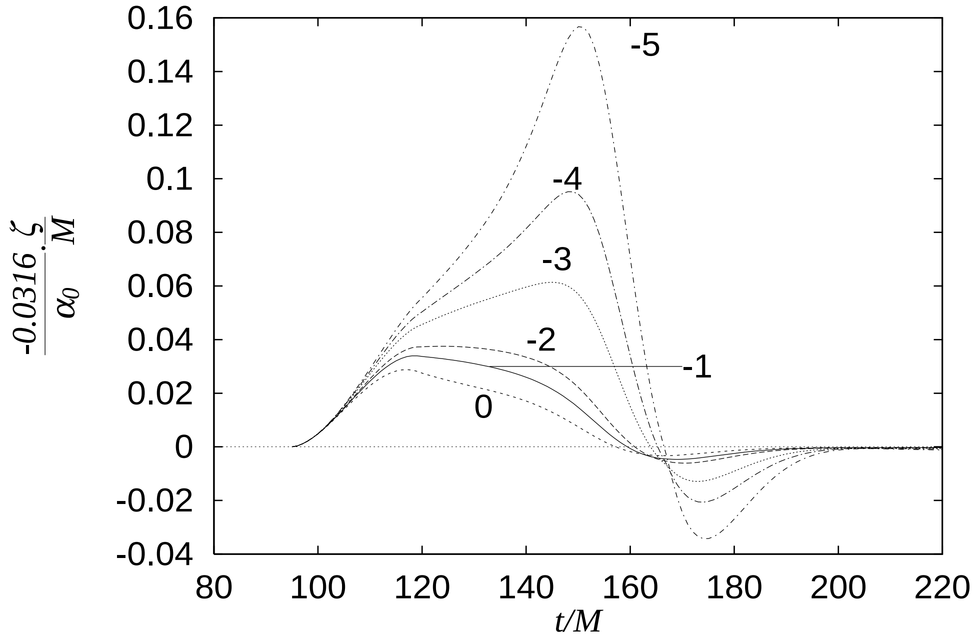
0.16
0.14
0.12
0.1
0.08
0.06
0.04
0.02
0
-0.02
-0.04
80
100
120
140
160
180
200
220
t/M
-5
-4
-3
-2
-1
0

Fig.12

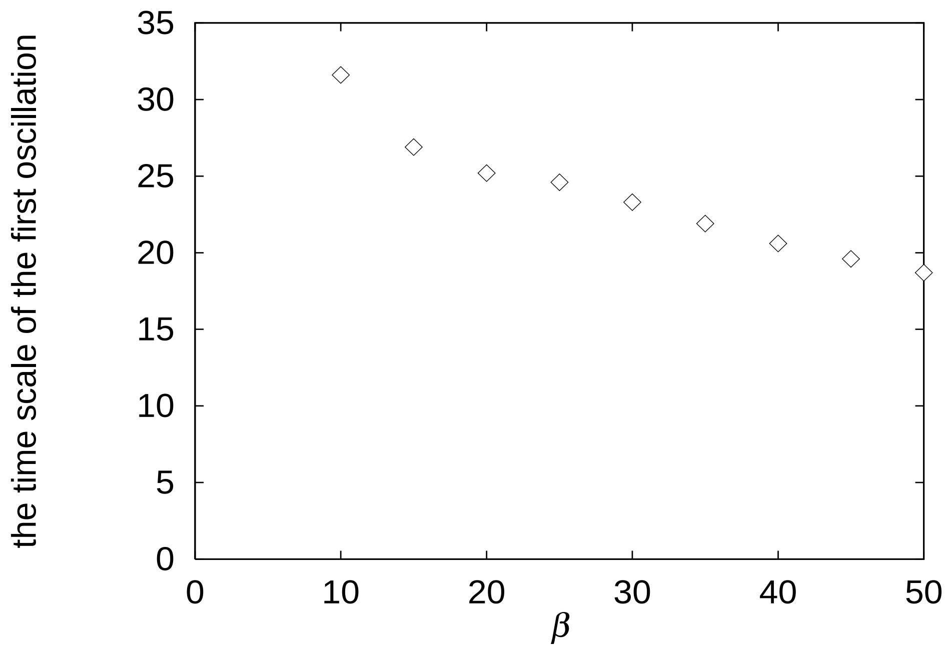
the time scale of the first oscillation
35
30
25
20
15
10
5
0
0
10
20
30
40
50
β

Fig.13

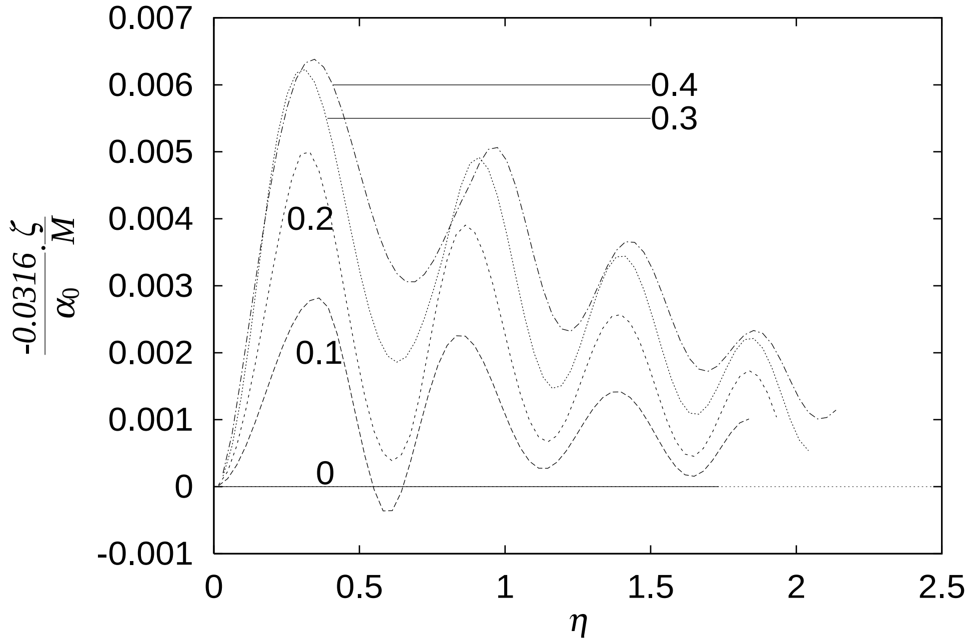
0.007
0.006
0.005
0.004
0.003
0.002
0.001
0
-0.001
0
0.5
1
1.5
2
2.5
$\eta$
$\frac{-0.0316}{\alpha_0} \cdot \frac{\zeta}{M}$
0.4
0.3
0.2
0.1
0

Fig.14

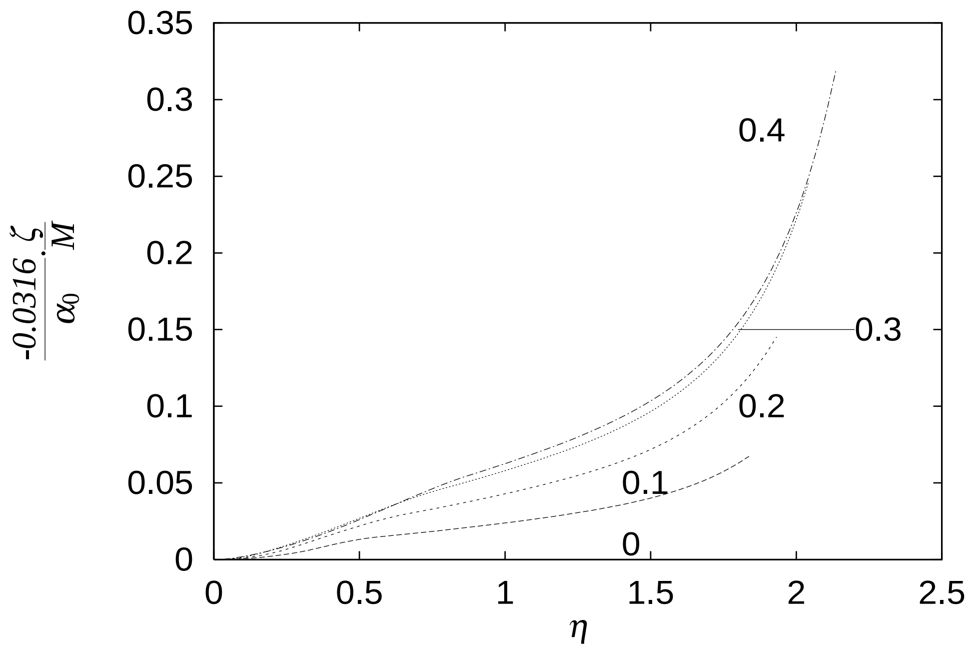
0.35
0.3
0.25
0.2
0.15
0.1
0.05
0
0
0.5
1
1.5
2
2.5
$\eta$
$\frac{-0.0316}{\alpha_0} \cdot \frac{\zeta}{M}$
0.4
0.3
0.2
0.1
0

Fig.15